Witnessing an extreme, highly efficient galaxy formation mode with resolved Lyman- α and Lyman-continuum emission

R. Marques-Chaves, D. Schaerer, E. Vanzella, A. Verhamme, M. Dessauges-Zavadsky, J. Chisholm, F. Leclercq, A. Upadhyaya, J. Álvarez-Márquez, L. Colina, et al.

A&A, 691, A87 (2024)
https://doi.org/10.1051/0004-6361/202451667

Astronomy & Astrophysics

Witnessing an extreme, highly efficient galaxy formation mode with resolved Lyman-α and Lyman-continuum emission

R. Marques-Chaves[1,⋆], D. Schaerer[1,2], E. Vanzella[3], A. Verhamme[1], M. Dessauges-Zavadsky[1], J. Chisholm[4], F. Leclercq[4], A. Upadhyaya[5], J. Álvarez-Márquez[6], L. Colina[6], T. Garel[1], and M. Messa[3]

[1] Department of Astronomy, University of Geneva, 51 Chemin Pegasi, 1290 Versoix, Switzerland
[2] CNRS, IRAP, 14 Avenue E. Belin, 31400 Toulouse, France
[3] INAF – OAS, Osservatorio di Astrofisica e Scienza dello Spazio di Bologna, via Gobetti 93/3, I-40129 Bologna, Italy
[4] Department of Astronomy, University of Texas at Austin, 2515 Speedway, Austin, Texas 78712, USA
[5] Department of Physics, University of Warwick, Gibbet Hill Road, Coventry CV4 7AL, UK
[6] Centro de Astrobiología (CAB), CSIC-INTA, Ctra. de Ajalvir km 4, Torrejón de Ardoz, E-28850 Madrid, Spain

Received 26 July 2024 / Accepted 6 September 2024

ABSTRACT

J1316+2614 at $z = 3.613$ is the UV-brightest ($M_{\rm UV} = -24.7$) and strongest Lyman continuum-emitting ($f_{\rm esc}^{\rm LyC} \approx 90\%$) star-forming galaxy known; it also shows signatures of inflowing gas from its blue-dominated Lyα profile. We present high-resolution imaging with the *Hubble* Space Telescope (HST) and the Very Large Telescope (VLT) of the LyC, Lyα, rest-UV, and optical emission of J1316+2614. Detailed analysis of the LyC and UV light distributions reveals compact yet resolved profiles, with LyC and UV morphologies showing identical half-light radii of $r_{\rm eff} \simeq 220$ pc. The continuum-subtracted Lyα emission, obtained with the HST ramp-filter *FR551N*, reveals an extended filamentary structure of ≃6.0 kpc oriented south to north with only residual flux within the stellar core, suggesting a Lyα 'hole'. Our spectral energy distribution analysis shows that J1316+2614 is characterised by a young (5.7 ± 1.0 Myr), nearly un-obscured stellar population with a high star-formation rate (SFR $= 898 \pm 181\ M_\odot\ {\rm yr}^{-1}$) and a stellar mass of $M_\star^{\rm young} = (4.8 \pm 0.3) \times 10^9\ M_\odot$. Additionally, the spectral energy distribution analysis supports the absence of an underlying old stellar population ($M_\star^{\rm old} \leq 2.8 \times 10^9\ M_\odot$, 3σ). J1316+2614 presents remarkably high SFR and stellar mass surface densities of $\log(\Sigma SFR[M_\odot\ {\rm yr}^{-1}\ {\rm kpc}^{-2}]) = 3.47 \pm 0.11$ and $\log(\Sigma M_\star[M_\odot\ {\rm pc}^{-2}]) = 4.20 \pm 0.06$, respectively, which are among the highest observed in star-forming galaxies and are more typically observed in local young massive star clusters and globular clusters. Our findings indicate that J1316+2614 is a powerful, young, and compact starburst that is leaking a significant amount of LyC photons due to a lack of gas and dust within the starburst. We explored the conditions for gas expulsion using a simple energetic balance and find that, given the strong binding force in J1316+2614, a high star-formation efficiency ($\epsilon_{\rm SF} \geq 0.7$) is necessary to explain the removal of gas and its exposed nature. Our results thus suggest a close link between high $\epsilon_{\rm SF}$ and high $f_{\rm esc}^{\rm LyC}$. This high efficiency can also naturally explain the remarkably high SFR, UV luminosity, and efficient mass growth of J1316+2614, which acquired at least 62% of its mass in the last 6 Myr. J1316+2614 may exemplify an intense, feedback-free starburst with a high $\epsilon_{\rm SF}$, similar to those proposed for UV-bright galaxies at high redshifts.

Key words. galaxies: high-redshift – galaxies: starburst – dark ages, reionization, first stars

1. Introduction

UV-bright star-forming galaxies were once considered extremely rare at any redshift, even at the epoch of re-ionisation (EoR; at $6 < z < 16$). However, recent *James Webb* Space Telescope (JWST) observations have dramatically changed this picture by revealing a large number of UV-bright and sometimes massive galaxies at $z \simeq 7-14$ (see e.g. Arrabal Haro et al. 2023; Bunker et al. 2023; Carniani et al. 2024; Castellano et al. 2024, for some spectroscopically confirmed sources). The derived volume densities of these sources exceed predictions from galaxy formation models and pre-JWST observations by an order of magnitude (e.g. Bouwens et al. 2021; Kannan et al. 2023; Lovell et al. 2023). These results are not in line with the common wisdom of galaxy formation and evolution, challenging our understanding of the nature of UV-bright galaxies and the potential role these sources play in cosmic re-ionisation.

Several scenarios have been proposed to explain this tension. One suggestion is that the star-formation efficiency (the efficiency in converting gas into stars; $\epsilon_{\rm SF}$) is higher than assumed in current models and measured locally (by a few percent; e.g. Megeath et al. 2016). In this framework (Dekel et al. 2023; Li et al. 2024; Boylan-Kolchin 2024), high-density environments and low metallicities, properties expected at early times, may favour the formation of so-called "feedback-free starbursts" (FFBs; Dekel et al. 2023) through the collapse of gas clouds within very short free-fall times. This would increase the star-formation efficiency since the cloud collapse occurs before the onset of strong feedback, thus also increasing star-formation rates (SFRs), UV luminosities, and stellar masses. Other works have related the excess of UV-bright sources to variations of the initial mass function (IMF) that allow the formation of more massive stars (e.g. Inayoshi et al. 2022; Finkelstein et al. 2023; Trinca et al. 2024). This excess of massive stars, also referred to as a "top-heavy" IMF, boosts the UV radiation and the luminosity-to-mass ratio, making these sources appear (UV-) brighter at fixed masses. On the other hand, Ferrara et al.

⋆ Corresponding author; rui.marquescoelhochaves@unige.ch

Table 1. HST and VLT imaging observations of J1316+2614.

Filter (1)	λ_{rest} [Å] (2)	t_{exp} [s] (3)	Scale [″/pix] (4)	PSF_{FWHM} [″] (5)	Mag. [AB] (6)	n (7)	b/a (8)	θ [deg] (9)	r_{eff} [pc] (10)
F410M	871–914	5004	0.0394	0.0745	23.32 ± 0.06	2.12 ± 0.91	0.71 ± 0.19	198 ± 36	262 ± 64
FR551N	1204–1225	2008	0.0500	0.1085	20.81 ± 0.10	–	–	–	–
F775W	1489–1859	2372	0.0396	0.0796	21.25 ± 0.04	2.90 ± 0.42	0.72 ± 0.05	162 ± 5	220 ± 12
F160W	3004–3686	2412	0.1272	0.1968	21.66 ± 0.05	–	–	–	≤442
K_s	4301–5003	1350	0.1065	0.2960	21.73 ± 0.06	–	–	–	≤550

Notes. (1) and (2) Filter and corresponding bandwidth in the rest-frame; (3) exposure time; (4) pixel scale; (5) PSF FWHM obtained from stars in the FoV; (6) aperture photometry of J1316+2614; (7) Sérsic index; (8) minor-to-major axis; (9); orientation (north = 0, east = 90); and (10) half-light effective radius.

(2023, see also Ziparo et al. 2023) propose that radiation-driven outflows originating from recent star formation could, for a limited time, remove dust as soon as it is produced. Dust ejection via strong radiative feedback would decrease the dust optical depth, making these galaxies appear brighter in the UV. Other frameworks invoke the stochastic nature of star formation at high redshifts (e.g. Mason et al. 2023; Shen et al. 2023), or even the contribution from active galactic nuclei (Hegde et al. 2024; Maiolino et al. 2024).

In parallel, extremely UV-bright star-forming galaxies at $z \simeq 2$–4 were discovered in the wide Sloan Digital Sky Survey by Marques-Chaves et al. (2020a, 2021, 2022). These galaxies present remarkably high UV absolute magnitudes of $M_{UV} \sim -24$ and are characterised by very young stellar populations (≤10 Myr) without signs of active galactic nucleus activity (based on the detection of photospheric absorption lines, wind line features, and UV/optical Baldwin-Phillips-Telervich diagrams). They show SFRs of up to SFR $\simeq 1000\,M_\odot\,yr^{-1}$ but also residual dust attenuation with UV continuum slopes as steep as $\beta_{UV} \simeq -2.6$ (e.g. Marques-Chaves et al. 2022). As such, these sources are among the most vigorous of the nearly un-obscured star-forming galaxies known, with specific star-formation rates (sSFRs) >50–100 Gyr^{-1}. Furthermore, they show complex gas kinematics, including outflows (Álvarez-Márquez et al. 2021; Marques-Chaves et al. 2021) and inflows (Marques-Chaves et al. 2022). The recent analysis of the rest-UV spectra of these sources by Upadhyaya et al. (2024) has revealed signatures of very massive stars (VMSs; with initial masses >100 $M_\odot$) for most of them, suggesting that VMSs might be common in UV-bright galaxies. Last but not least, the two sources with Lyman continuum (LyC) observations identified so far, J0121+0025 ($z = 3.2$) and J1316+2614 ($z = 3.6$), show copious LyC leakage, with absolute escape fractions of up to $f_{esc}^{LyC} \approx 90\%$ (Marques-Chaves et al. 2021, 2022). As the UV-brightest star-forming galaxies known, they are ideal laboratories for testing the various scenarios proposed to explain the overabundance of UV-bright EoR sources.

We present high-spatial-resolution observations of J1316+2614 at $z = 3.61$ (Marques-Chaves et al. 2022), the UV-brightest star-forming galaxy ($M_{UV} = -24.7$) detected so far, and also the strongest LyC emitter known ($f_{esc}^{LyC} \simeq 90\%$). J1316+2614 is a powerful starburst with negligible dust attenuation, as evidenced by its steep UV slope ($\beta_{UV} = -2.59 \pm 0.05$). It shows relatively weak nebular emission (e.g. $EW_0(H\beta) = 34.7 \pm 6.8$ Å) due to the high fraction of ionising photons escaping its interstellar medium (ISM; $f_{esc}^{LyC} \approx 90\%$ and $\log(Q_H^{esc}/s^{-1}) = 55.86 \pm 0.11$; Marques-Chaves et al. 2022). Finally, J1316+2614 also shows a peculiar Lyman α (Lyα) spectral profile with a blue-to-red peak line ratio of $I_{blue}/I_{red} \simeq 3.7$, which suggests the presence of inflows.

This work is organised as follows. In Sect. 2 we describe high-resolution observations taken with the *Hubble* Space Telescope (HST) and the Very Large Telescope (VLT) probing the LyC, Lyα, rest-UV, and optical emission of J1316+2614. In Sect. 3 we describe our methodology and present our main results, including the morphology, photometry, and the spectral energy distribution (SED) of J1316+2614. We present a discussion of the results in Sect. 4 and a summary of our main findings in Sect. 5. Throughout this work, we use a concordance cosmology with $\Omega_m = 0.274$, $\Omega_\Lambda = 0.726$, and $H_0 = 70\,km\,s^{-1}\,Mpc^{-1}$. Magnitudes are given in the AB system.

2. Observations

2.1. HST imaging

High-resolution imaging of J1316+2614 was obtained with the UVIS/IR imager Wide Field Camera 3 (WFC3) and the Advanced Camera for Surveys (ACS) of the Wide Field Channel (WFC) aboard the HST. These observations were carried out between June 26 and July 3, 2023, under Cycle 30 programme 17286 (PI: R. Marques-Chaves). J1316+2614 was observed with the WFC3 in the medium-band *F410M* and broadband filters *F775W* and *F160W*, with total exposure times of 5004 s, 2372 s, and 2412 s, respectively. These filters probe the rest-frame LyC (≃871–914 Å)[1], UV (≃1650 Å), and optical (≃3310 Å) emission of J1316+2614. Additional ACS/WFC observations were obtained with the narrow-band ramp filter *FR551N* (transmission width of ≃97 Å) centred at $\lambda_{obs} = 5604$ Å to cover the Lyα emission of J1316+2614 at $z = 3.612$. The ACS total exposure time was 2008 s. Table 1 summarises the HST observations.

The data were reduced using `AstroDrizzle` version 3.6.2 from the `DrizzlePac` package (Fruchter & Hook 2002) and retrieved from MAST. The final images have pixel scales of 0.04″ pix^{-1} (*F410M* and *F775W*), 0.05″ pix^{-1} (*FR551N*), and 0.12″ pix^{-1} (*F160W*). The astrometry was corrected and aligned to the *Gaia* Data Release 3 (DR3; Gaia Collaboration 2023). The astrometry r.m.s precision is ≃0.09″–0.12″. The instrumental point-spread function (PSF) in each image was modelled using the point-spread function reconstruction (`PSFr`; Birrer et al. 2021, 2022) code by stacking several (three to five) isolated bright stars within the field of view (FoV) of the observations. We measure PSF full widths at half maximum (FWHMs) of

[1] The *F410M* filter response at $\lambda_0 > 912$ Å is less than ∼0.08, and therefore, the contamination of non-LyC emission in *F410M* is negligible (e.g. Smith et al. 2018).

0.075″, 0.109″, 0.080″, 0.197″ for $F410M$, $FR551N$, $F775W$, and $F160W$, respectively. Figure 1 shows the $F775W$ image of J1316+2614 and the contours from $F410M$.

2.2. VLT/HAWK-I imaging

Additional near-IR imaging of J1316+2614 was obtained in the K_s band with the HAWK-I on the VLT UT4. These observations were conducted on May 31, 2023, as part of programme 111.251K.001 (PI: R. Marques-Chaves). K_s-band observations were obtained with the GRound layer Adaptive optics system Assisted by Lasers (GRAAL), enhancing the final image quality down ≃0.296″, as measured from the light profiles of several stars in the HAWK-I FoV. The on-source exposure time was 1350 s. The data were reduced using the standard ESO pipeline version 2.4.12[2] and were flux calibrated against 2MASS stars in the field. The astrometry was calibrated using the *Gaia* DR3 catalogue (Gaia Collaboration 2023) yielding an r.m.s precision of ≃0.10″, similar to the native pixel scale (0.107″).

3. Methodology and results

3.1. Size measurements

As shown in Fig. 2, the HST and VLT images reveal a compact morphology in the bands probing the stellar continuum of J1316+2614 ($F410M$, $F775W$, $F160W$, and K_s). In contrast, the ACS/$FR551N$ image, which predominantly traces the Lyα emission, shows a well-resolved and extended profile.

3.1.1. Stellar morphology

The light distribution of J1316+2614 is investigated using the `PySersic` code (Pasha & Miller 2023), which uses a Bayesian framework to understand the degeneracies between different parameters. `PySersic` fits the light distribution of a source using morphological models convolved with a given PSF. As described in Sect. 2, the PSF of each image is obtained by stacking several bright stars within the FoV using the `PSFr` code (Birrer et al. 2021, 2022). We fitted the morphology of J1316+2614 using both 2D Sérsic (with a Sérsic index varying from 0.5 to 6.0) and point-like profiles to investigate whether the light distribution of J1316+2614 is resolved in each band.

We started fitting the light profile of J1316+2614 using the HST $F775W$ (rest-UV). Assuming a Sérsic profile, `PySersic` finds an effective radius $r_{\rm eff} = 0.76 \pm 0.04$ pix (or $r_{\rm eff} = 220 \pm 12$ pc with our adopted cosmology) and a Sérsic index $n = 2.90 \pm 0.42$. The normalised residuals (NR), measured within a circular aperture of 0.6″ around J1316+2614, are NR ≃ 8% (Fig. 3). While a Sérsic profile recovers most (≳90%) of the light emission in $F775W$, the model-subtracted image shows some residuals that are not perfectly accounted for and suggest additional underlying structures. If instead a point-like profile is used in the fit, `PySersic` cannot recover the light profile of J1316+2614 well and leaves substantial residuals in the model-subtracted image (NR ≃ 22%; right-middle panel of Fig. 3). Our results thus indicate that J1316+2614 has a resolved morphology in the rest-UV continuum ($r_{\rm eff} = 220 \pm 12$ pc), as also indicated through its radial profile (bottom panel of Fig. 2).

[2] https://www.eso.org/sci/software/pipelines/hawki/hawki-pipe-recipes.html.

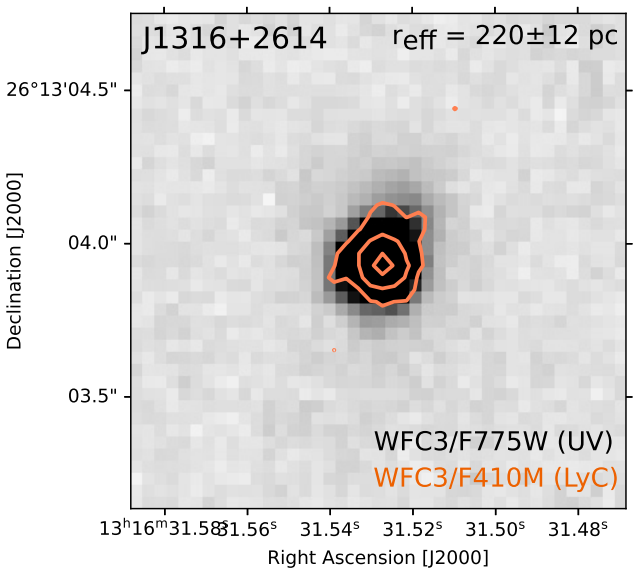

Fig. 1. Cutout image of J1316+2614 showing the HST $F775W$ (background image) and $F410M$ (orange contours, 5σ, 10σ, and 50σ) images, which probe the rest-UV and LyC emission of J1316+2614, respectively.

Similar to $F775W$, the profile of J1316+2614 in the HST $F410M$ (LyC) appears resolved. Assuming a Sérsic profile, the `PySersic` best-fit predicts an effective radius $r_{\rm eff} = 0.79 \pm 0.21$ pix or $r_{\rm eff} = 262 \pm 64$ pc and a Sérsic index $n = 2.12 \pm 0.91$. The normalised residuals from this fit, measured within $r \leq 0.6''$), are significantly better (≃7%) than those obtained assuming a point-like source (≃28%, Fig. 3). This suggests that the LyC emission seen in $F410M$ is resolved and has a similar morphology to the rest-UV emission. To investigate this, we inspected the residuals obtained from the PSF-subtracted images. As shown in Fig. 3, the PSF-subtracted images in $F410M$ and $F775W$ show almost identical residuals (highlighted with blue arrows), indicating that the even faintest resolved emission in $F775W$ is present in $F410M$. In addition, we inspected the $F410M$ and $F775W$ normalised radial profiles of J1316+2614 and find that they are indistinguishable within the uncertainties (Fig. 2). Finally, we modelled the $F410M$ emission using the $F775W$ image of J1316+2614 as a PSF and assuming a point-like source. The normalised residuals are slightly better than the ones obtained assuming a Sérsic model. Altogether, our results indicate that the LyC ($F410M$) and rest-UV ($F775W$) light profiles of J1316+2614 are essentially the same, and consistent with $r_{\rm eff} = 220$ pc. This strongly supports that the LyC and UV emissions have similar origins.

Turning to longer wavelengths, the light distribution of J1316+2614 in the HST $F160W$ and VLT K_s bands appears unresolved. This is expected given the slightly poorer spatial resolution in these bands and the fact that they still probe the young stellar population of J1316+2614 ($r_{\rm eff} \simeq 220$ pc). Our best-fit models assuming Sérsic or point-like profiles yield essentially similar residual images. Given the oversampling of the HST/$F160W$ PSF (FWHM ≃ 1.6 pix), we used the minimum resolvable size of $r_{\rm eff} \leq 0.47$ pix estimated in Messa et al. (2022) for the same instrument and filter considered here to infer the upper limit $r_{\rm eff} \leq 442$ pc in the HST/$F160W$. Since the HAWK-I PSF is well sampled (FWHM ≃ 2.8 pix), we derive an upper limit in the K_s band of $r_{\rm eff} \leq 550$ pc assuming FWHM$_{\rm min} \leq$ FWHM(PSF)/2.

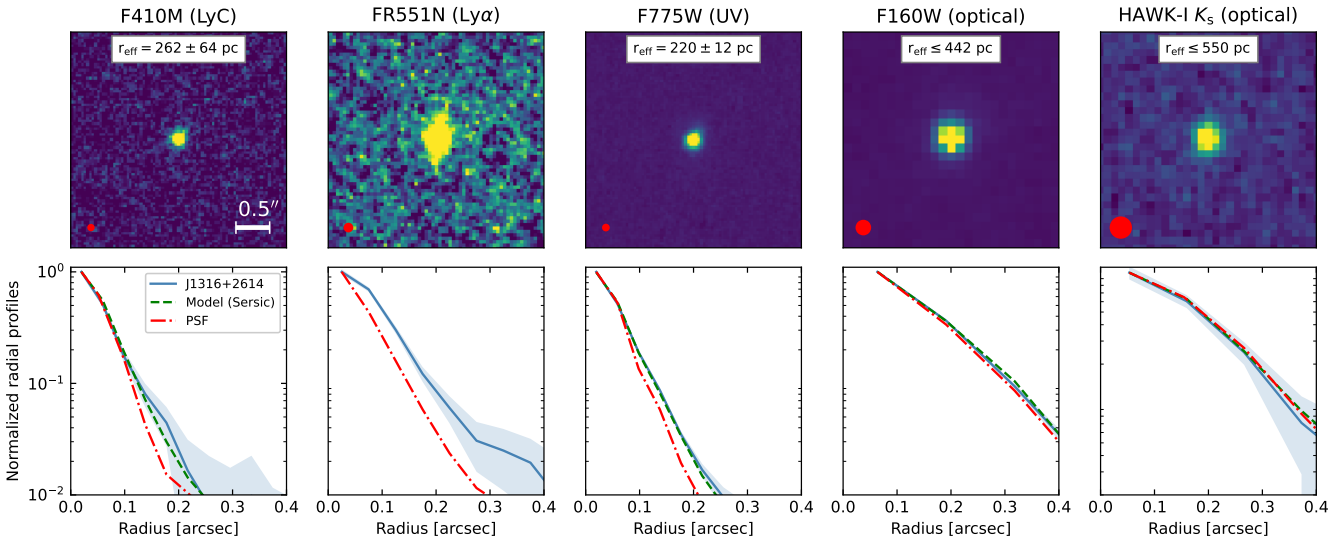

Fig. 2. HST and VLT images of J1316+2614. From left to right: HST *F*410*M* (LyC), *FR*551*N* (Lyα), *F*775*W* (rest-UV), *F*160*W* (rest-optical), and VLT HAWK-I K_s (rest-optical) images. The FWHM PSF of an image is represented with a red circle. Each stamp has a size of 3.2″ × 3.2″. North is up, and east is to the left. Bottom panels: Normalised (to their maxima) radial profiles of J1316+2614 in each band (solid blue, with uncertainties shown as the shadow), the best-fit Sérsic model (dashed green), and the PSF used in the fit (dotted dashed red). J1316+2614 shows a compact stellar morphology only in the *F*410*M* and *F*775*W* images ($r_{\rm eff} \simeq 220$ pc). The *FR*551*N* filter, which probes the Lyα emission (and stellar continuum), detects a more extended morphology.

3.1.2. Lyα morphology

Finally, we analysed the HST ACS/*FR*551*N* image of J1316+2614, which includes the Lyα emission ($EW_0 = 20.5 \pm 1.9$ Å; Marques-Chaves et al. 2022). As shown in the top-left panel of Fig. 4, the ACS/*FR*551*N* image reveals a complex morphology consisting of a bright central clump co-spatial with the compact stellar emission (e.g. as seen in *F*410*M* or *F*775*W*) and a more diffuse, filamentary-like emission oriented south to north with a 3σ scale length of ≃0.8″ or ≃6.0 kpc.

We employed two different methodologies to subtract the underlying stellar emission in the *FR*551*N* band. For the first one (method 1 in Fig. 4), we used the WFC3/*F*775*W* as the reference image of the stellar emission of J1316+2614, which was first resampled to the *FR*551*N* native pixel size (0.05″ pix^{-1}) using the `MAGNIFY` task from `Iraf`. We repeated this step in an individual star and find no significant differences between the PSF FWHM measured in *FR*551*N* and the resampled *F*775*W* images. Since the astrometry uncertainties in both filters (≃0.10″) are larger than the pixel size, we chose to spatially match both images of J1316+2614 using their centroid emission and the corresponding shifts in pixels using the `Iraf` task `imshift`. This step assumes that the centroid emission in *FR*551*N* is dominated by the stellar continuum, which is a fair assumption since the continuum emission represents ≃50% of the total flux in *FR*551*N* (see next) and is far more compact than the extended Lyα emission. We infer the contribution of the stellar continuum in the *FR*551*N* passband using the low-resolution optical spectrum of J1316+2614 obtained with GTC/OSIRIS, which was previously rescaled to the *R*-band photometry to account for slit losses (see Marques-Chaves et al. 2022). As highlighted in the top-right panel of Fig. 4, the contribution of the stellar emission is obtained by fitting a linear polynomial function using two spectral windows on each side of Lyα (5480–5527 Å and 5757–5841 Å). Using `PyPhot`[3] and the *FR*551*N* transmission profile centred at $\lambda = 5604$ Å, we measured the synthetic photometry of the polynomial function, which probes only the stellar continuum. We find $f_\nu^{\rm cont} \simeq 9.62 \times 10^{-29}$ erg s^{-1} cm^{-2} Hz^{-1}, which represents roughly ≃50% of the total emission in *FR*551*N*. Finally, we rescale the flux of the resampled *F*775*W* image to that obtained from the synthetic photometry and subtract it from the *FR*551*N* image.

The bottom-left panel of Fig. 4 shows the continuum-subtracted *FR*551*N* image (method 1), that is, the Lyα emission of J1316+2614. As seen in this figure, Lyα is predominantly emitted in the outskirts of the UV-bright stellar core, whose total size is represented by an orange circle with a radius of $2 \times r_{\rm eff}$ (≃ 0.06″). This bright UV continuum in the centre of the galaxy leads to a Lyα hole with weak/residual Lyα emission being emitted at the position of the stellar core. It is important to note that the continuum-subtracted Lyα image, especially its faint and diffuse emission, is affected by additional noise due to the subtraction process of the *F*775*W* image from the *FR*551*N* image.

For consistency, we explore an alternative method for subtracting the stellar contribution in *FR*551*N* (method 2 in Fig. 4). Using `PySersic`, we model a Sérsic profile with the best-fit parameters obtained for the stellar continuum in *F*775*W* (i.e. $r_{\rm eff} = 220$ pc, $n = 2.90$, Table 1) and convolved it with the PSF of *FR*551*N* obtained from stars in the FoV. After rescaling the flux, we subtract this model from the *FR*551*N* image. Consistent with our previous method, we recover the weak/residual Lyα emission within the stellar core. However, we note that the spatial distribution of the bright Lyα emission around the stellar component differs slightly from the previous method, as seen in the bottom panels of Fig. 4. Lastly, we investigate the uncertainties on the assumed flux and contribution of the stellar continuum in *FR*551*N*. We repeat our analysis, conservatively assuming a stellar contribution in *FR*551*N* of ≃40%. Under this assumption, the Lyα 'hole' appears less prominent but is still present, with the bulk of Lyα photons emitted around (and far away) from the stellar core.

While a detailed characterisation of this hole (e.g. its size) is difficult and requires deeper data, given the low significance of the Lyα emission and other uncertainties in our methodology,

[3] https://github.com/mfouesneau/pyphot

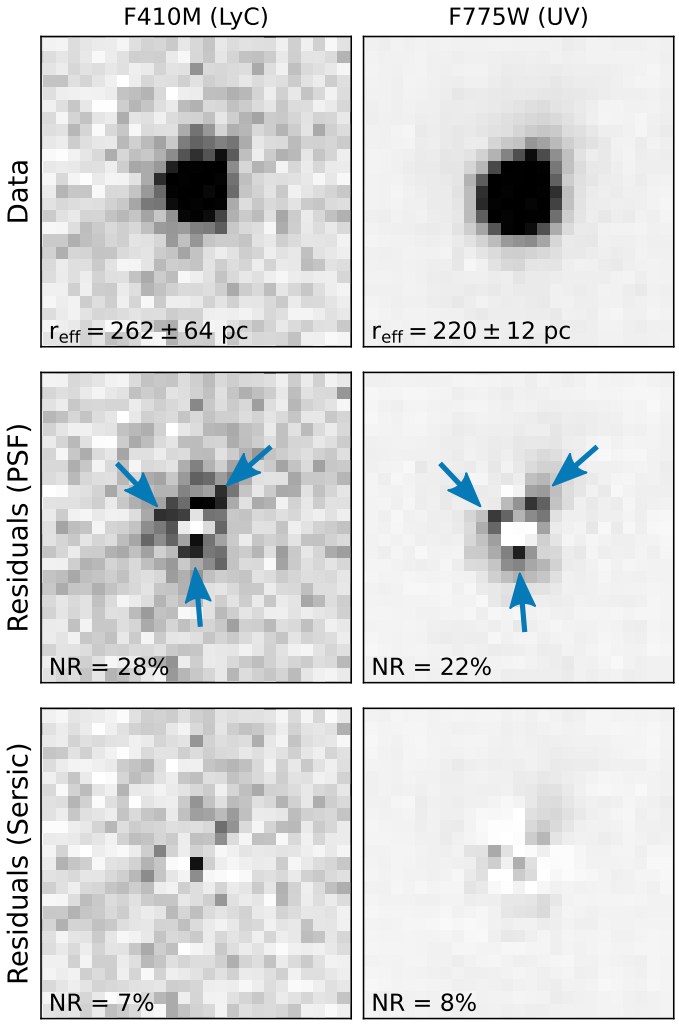

Fig. 3. HST $F410M$ (LyC; left) and $F775W$ (UV; right) images of J1316+2614 (top) and the residuals obtained after subtracting the PSF and Sérsic best-fit models (middle and bottom, respectively). The normalised residuals (NR), measured in a circular aperture of 0.6″ around J1316+2614, are also indicated. Each stamp has a size of 1.0″ × 1.0″. North is up, and east is to the left. The PSF-subtracted residuals are identical in the $F410M$ and $F775W$ images, indicating similar LyC and rest-UV morphologies.

our results strongly support a deficit of Lyα co-spatial with the stellar continuum. Such a configuration was discussed and predicted in Marques-Chaves et al. (2022) in order to reconcile the high $f_{\rm esc}^{\rm LyC} \simeq 90\%$, requiring a gas column density $N_{\rm HI} \lesssim 10^{17}\,{\rm cm}^{-2}$, and the large Ly$\alpha$ velocity peak separation observed in J1316+2614 ($\Delta v = 680 \pm 70\,{\rm km\,s}^{-1}$), which suggests $N_{\rm HI} \sim 10^{21}\,{\rm cm}^{-2}$ according to the radiative models of Verhamme et al. (2015) under standard conditions. We further discuss the connection between the Lyα and LyC-UV spatial distributions in Sect. 4.2.

3.2. Photometry

Using `Sextractor` (Bertin 2006) we performed aperture photometry on J1316+2614 assuming an aperture of 0.8″ diameter. For $F410M$, we measure $F410M = 23.32 \pm 0.06$, which is in excellent agreement with that inferred from the optical GTC/OSIRIS spectrum presented in Marques-Chaves et al. (2022, 23.33±0.06). Similarly, we obtain $F775W = 21.25 \pm 0.04$ and $F160W = 21.66 \pm 0.05$, which is consistent with previous ground-based photometry probing similar spectral ranges ($I = 21.24 \pm 0.08$ and $H = 21.70 \pm 0.14$; Marques-Chaves et al. 2022). For the HAWK-I $K_{\rm s}$ band, we measure $K_{\rm s} = 21.73 \pm 0.06$, which is substantially different than that obtained with GTC/EMIR ($K_{\rm s} = 21.31 \pm 0.07$). These differences are likely due to the shorter spectral coverage of the HAWK-I $K_{\rm s}$ band ($\lambda = 1.984{-}2.308\,\mu{\rm m}$) compared to the GTC/EMIR one ($\lambda = 2.080{-}2.388\,\mu{\rm m}$), meaning the former does not include the contribution of the redshifted [O III] λ5008 emission ($\lambda \simeq 2.310\,\mu{\rm m}$). The ACS/$FR551N$ image of J1316+2614 shows a more extended profile due to the Lyα emission, as shown in Fig. 2. Given its extended emission, we used a large aperture of 1.2″ diameter, obtaining $FR551N = 20.81 \pm 0.10$. Table 1 summarises the photometry of J1316+2614.

In addition to the photometry of the UV-bright and compact starburst, we constrained the flux densities of an underlying stellar population in J1316+2614. The SED analysis by Marques-Chaves et al. (2022) using unresolved photometry supports the absence of a significant old stellar population. We assumed that the underlying old stellar population has a Gaussian profile with an effective radius of 1.5 kpc centred at the position of the UV-bright emission. This size assumption was motivated by the characteristic effective radius of Lyman-break galaxies ($r_{\rm eff}^{\rm LBGs} \simeq 1.3$ kpc; e.g. Ribeiro et al. 2016) and the size of the dust emission of J1316+2614 detected by ALMA ($r_{\rm eff}^{\rm dust} \simeq 1.7$ kpc), which could already be produced before the UV-bright starburst in J1316+2614 (as discussed in Dessauges-Zavadsky et al., in prep.). Given the fact that J1316+2614 is unresolved in the HST/$F160W$ and VLT/$K_{\rm s}$ images (Sect. 3.1), we thus simulated the maximum flux of the underlying stellar population needed to resolve the total emission in these bands. While it is more extended than the UV-bright component, we find that the underlying old population should be fainter than $F160W > 24.95$ and $K_{\rm s} > 23.98$ to keep the total emission unresolved in $F160W$ and $K_{\rm s}$, respectively.

3.3. Spectral energy distribution

Using the photometry from the new images along with the previous ones obtained and discussed in Marques-Chaves et al. (2022), we re-analysed the SED of J1316+2614. Following Marques-Chaves et al. (2022), we performed SED-fitting with `CIGALE` version 2022.1 (Burgarella et al. 2005; Boquien et al. 2019) using the available photometry and flux measurements of the Hβ and [O III] $\lambda\lambda$4960,5008. Two stellar components were assumed to probe the young UV-bright starburst (assuming a constant star-formation history), and we used a burst model with an age of 1.4 Gyr to probe the maximum light and mass of an underlying, old stellar population, which corresponds to a formation redshift of ≃12.5. We assumed the Calzetti et al. (2000) dust attenuation law and the Chabrier (2003) IMF. Stellar population models from Bruzual & Charlot (2003) with the metallicity of $Z = 0.008$ were used (Marques-Chaves et al. 2022). We also left $f_{\rm esc}^{\rm LyC}$ as a free parameter.

Overall, the properties of the UV-bright starburst obtained from `CIGALE` agree with those previously derived in Marques-Chaves et al. (2022). Figure 5 shows the best-fit SED of J1316+2614. The UV-bright starburst is characterised by a young stellar population with an age of 5.7 ± 1.0 Myr and a continuous SFR = 898 ± 181 $M_\odot\,{\rm yr}^{-1}$ with residual dust attenuation ($E(B-V) = 0.03 \pm 0.01$). The SFR derived here reflects the total SFR within 5.7 Myr (i.e. the age of the young

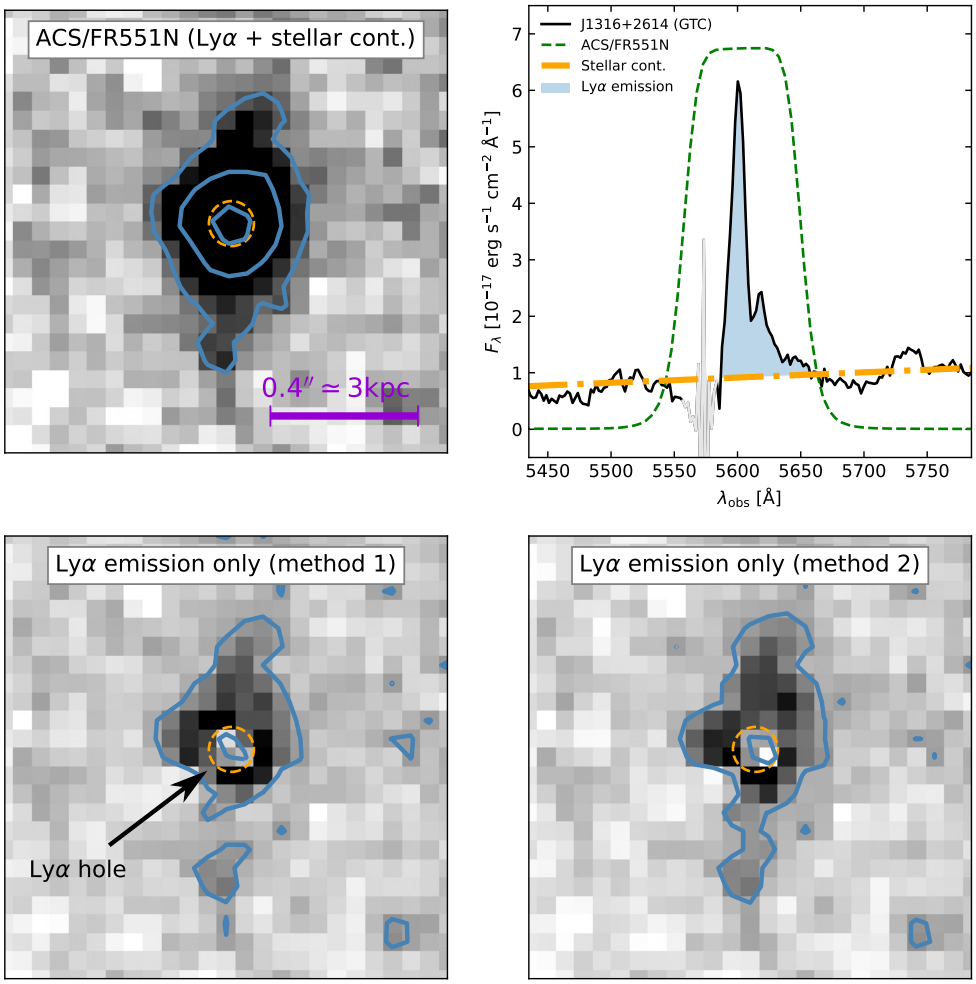

Fig. 4. Lyα spatial distribution of J1316+2614. Top left: Cutout images of J1316+2614 in the ACS/HST ramp-filter *FR551N* (with a total size of 1.2″ × 1.2″; north is up, and east to the left), which includes the Lyα emission and the underlying stellar continuum (blue contours mark the 3σ, 15σ, and 50σ emission). The dashed orange circle represents the position and total size of the stellar continuum as measured in the *F775W* and deconvolved with the PSF (i.e. a radius of $2 \times r_{\rm eff} \simeq 0.06''$). Top right: GTC spectrum of J1316+2614 (black; Marques-Chaves et al. 2022) and the *FR551N* transmission curve (dashed green). The dashed-dotted orange line represents our best fit of the stellar continuum around the Lyα emission (blue). Bottom panels: *FR551N* images continuum-subtracted using two different methods (see the main text). Lyα appears residual within the UV-bright stellar clump (orange) and is predominantly emitted in the outskirts. The blue contours mark the 2.5σ level.

stellar population). If instead we use the 10 Myr-weighted SFR indicator, we obtain SFR = 492 ± 35 $M_\odot$ yr^{-1}, which is consistent with the value reported in Marques-Chaves et al. (2022), SFR = 496 ± 92 $M_\odot$ yr^{-1}. The mass formed in this young starburst is $\log(M_\star^{\rm young}/M_\odot) = 9.68 \pm 0.03$, in excellent agreement with previous measurements ($\log(M_\star^{\rm young}/M_\odot) = 9.67 \pm 0.07$; Marques-Chaves et al. 2022). Our best-fit model also predicts $f_{\rm esc}^{\rm LyC} = 0.75 \pm 0.16$.

On the other hand, the new and deeper photometry in HST/*F160W* and VLT/$K_{\rm s}$ presented in this work, which probes the rest-optical stellar continuum, provides significantly improved constraints on the properties of the old stellar population. Our best-fit model predicts an old stellar component, assumed here as a 1.4 Gyr old burst model, with a stellar mass of $\log(M_\star^{\rm old}/M_\odot) = 9.00^{+0.29}_{-1.36}$ or $\log(M_\star^{\rm old}/M_\odot) \leq 9.46$ (3σ). The strong constraints on the mass of the old stellar component are due to the fact that the HST/*F160W* and VLT/$K_{\rm s}$ photometry is fully dominated by the starlight from the young starburst, leaving minimal room for an additional, older stellar component.

In short, our results strongly support that the extremely UV-bright starburst not only dominates the rest-UV and optical light emission of J1316+2614 (≃100%) but also its stellar mass, with a mass fraction of the galaxy formed in the last ≃6 Myr of $f_{\rm burst} = M_\star^{\rm young}/(M_\star^{\rm young} + M_\star^{\rm old}) \geq 62\%$ (3σ). We further discuss the implications of these findings in Sect. 4.5.

4. Discussion

4.1. J1316+2614 with cluster-like surface densities

J1316+2614 is the UV-brightest star-forming galaxy known ($M_{\rm UV} = -24.7$) and one of the most compact. Using the derived mass and SFR from Sect. 3.3, along with its size ($r_{\rm eff} = 220 \pm 12$ pc), we measured the stellar mass and SFR surface densities, defined as $\Sigma M_\star = M_\star/(2\pi r_{\rm eff}^2)$ and $\Sigma SFR = SFR/(2\pi r_{\rm eff}^2)$. J1316+2614 shows remarkably high mass and SFR surface densities of $\log(\Sigma M_\star[M_\odot\,{\rm pc}^{-2}]) = 4.20 \pm 0.06$ and $\log(\Sigma SFR[M_\odot\,{\rm yr}^{-1}\,{\rm kpc}^{-2}]) = 3.47 \pm 0.11$, respectively. Figure 6 shows the position of J1316+2614 (blue star) in the mass (top) and SFR (middle) versus $r_{\rm eff}$ diagrams. For comparison, similar measurements are provided for various compilations of galaxies at $z \simeq 1-5$ (red: van der Wel et al. 2012),

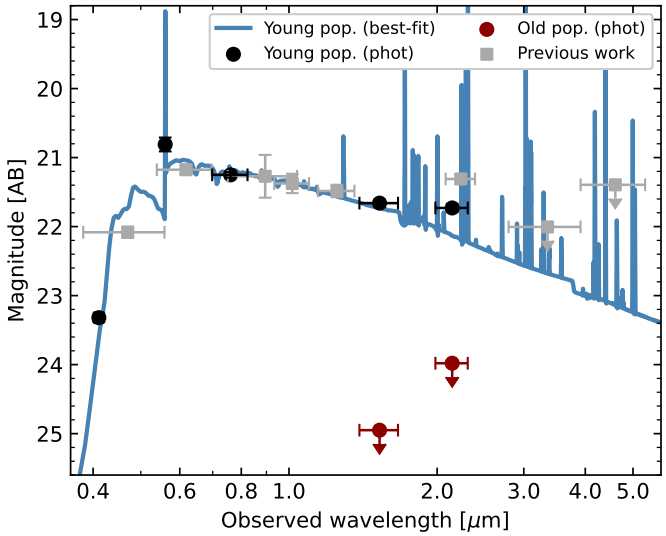

Fig. 5. Best-fit SED model (blue) of J1316+2614. The fit uses the new photometry obtained with HST and VLT (black circles) and the one presented in Marques-Chaves et al. (2022, grey squares). The SED of J1316+2614 is dominated by a young stellar population with an age of 5.7 ± 1.0 Myr and a continuous SFR of $898 \pm 181\ M_\odot\ \mathrm{yr}^{-1}$. The mass formed in this starburst is $\log(M_\star^{\mathrm{young}}/M_\odot) = 9.68 \pm 0.03$ with a residual dust attenuation ($E(B-V) = 0.03 \pm 0.01$). The red upper limits represent the maximum flux of the underlying stellar population needed to resolve the emission in the $F160W$ and K_s bands (see Sect. 3.2).

star-forming clumps in lensed galaxies (green: Claeyssens et al. 2023; Fujimoto et al. 2024; Messa et al. 2024), star-clusters and young massive clusters at different redshifts (yellow: Norris et al. 2014; Vanzella et al. 2023; Adamo et al. 2024), and local globular clusters, ultracompact dwarfs, and compact elliptical galaxies from (Norris et al. 2014, orange).

As shown in Fig. 6, the $\Sigma M_\star$ and ΣSFR of J1316+2614 deviate considerably from those of $z \simeq 1$–5 galaxies, by approximately 1–4 dex on average. At these redshifts, star-forming galaxies with high ΣSFR are indeed extremely rare, with very few dusty sub-millimetre-selected galaxies with ΣSFR values approaching those of J1316+2614 (Oteo et al. 2017). In addition, very few galaxies exhibit similar $\Sigma M_\star$, such as ultracompact dwarfs (e.g. M32) and compact elliptical galaxies in the local Universe (Norris et al. 2014), or extremely massive and compact quiescent galaxies at $z \sim 2$–5 (e.g. van Dokkum et al. 2008; Barro et al. 2017; de Graaff et al. 2024; Glazebrook et al. 2024). However, these evolved galaxies have residual star formation. At higher redshifts ($z > 5$), star-forming galaxies tend to show higher $\Sigma M_\star$ and ΣSFR than their lower-z counterparts, as recently shown by Langeroodi & Hjorth (2023) and Morishita et al. (2024). Still, even the densest sources at $z > 5$ struggle to reach the densities observed in J1316+2614 (bottom panel in Fig. 6). To our knowledge, only a few star-forming galaxies at $z > 6$ show comparable densities to J1316+2614 (Bunker et al. 2023; Williams et al. 2023; Castellano et al. 2024; Schaerer et al. 2024a; Topping et al. 2024; Álvarez-Márquez et al., in prep.), several of them are UV-bright and exhibiting peculiar abundance patterns resembling those seen in globular clusters (Charbonnel et al. 2023; Marques-Chaves et al. 2024; Schaerer et al. 2024a; Senchyna et al. 2024).

The densities derived for J1316+2614 are indeed extreme in star-forming galaxies, and more closely resemble those observed in young massive stellar clusters, which are among the densest systems known (Fig. 6). Following Kruijssen (2012),

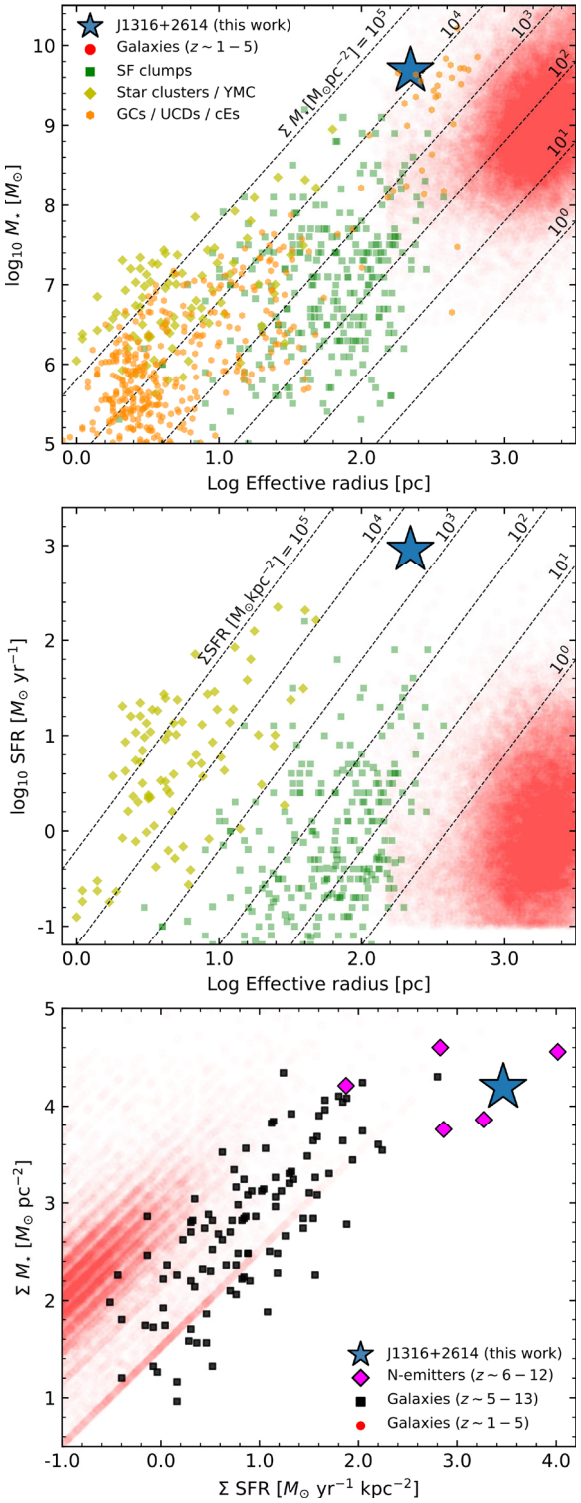

Fig. 6. Stellar mass (top) and SFR (middle) as a function of effective radius. J1316+2614 is represented with a blue star. Measurements of other compilations of galaxies at $z = 1$–5 (red circles; van der Wel et al. 2012), star-forming clumps in lensed galaxies (green squares; Claeyssens et al. 2023; Fujimoto et al. 2024; Messa et al. 2024), and star clusters and YMCs at different redshifts (yellow diamonds; Norris et al. 2014; Vanzella et al. 2023; Adamo et al. 2024) are also shown. For star clusters and star-forming clumps without SFR measurements, we assume star-formation ages of 1 Myr and 10 Myr, respectively, and SFR = $M_\star$/age. Bottom: $\Sigma M_\odot$ vs. ΣSFR of J1316+2614 along with other galaxies at higher redshifts (black), including very compact sources with strong nitrogen emission (violet) that exhibit abundance patterns resembling those seen in globular clusters.

J1316+2614 would have a very high cluster formation efficiency, $\Gamma \simeq 85\%$, given its high ΣSFR. However, while the surface densities of J1316+2614 are similar to those of massive star clusters, its starburst mass and UV-luminosity differ significantly ($\gtrsim$3−5 dex). It remains unclear whether J1316+2614 consists of a large number of normal star clusters ($N \sim 5\times10^4$ clusters with $10^5\,M_\odot$ each) compacted in a ~220 pc radius, or if its luminosity and mass originate from a single, supermassive star cluster with a total mass $M_\star \sim 5\times10^9\,M_\odot$.

4.2. Spatially resolved LyC and gas distributions

J1316+2614 represents the first example of resolved LyC in a strong LyC emitter star-forming galaxy (see also Meštrić et al. 2023 for resolved LyC in a star cluster). As shown in Sect. 3.1.1 and highlighted in Fig. 7, the LyC emission is not only resolved but its size and morphology are remarkably similar to that of the non-ionising UV (with $r_{\rm eff} \simeq 220$ pc). This is further highlighted in the bottom-right panel of Fig. 7, where the LyC and UV (normalised) radial profiles are shown (black and yellow, respectively). Despite potential variations in the PSF between $F410M$ and $F775W$, which are residual (Table 1) and were accounted for in our morphological analysis with `PySersic` (Sect. 3.1.1), the figure shows that the LyC and UV radial profiles are indistinguishable within the uncertainties. Together with the high $f_{\rm esc}^{\rm LyC} \approx 90\%$ measured in Marques-Chaves et al. (2022), the almost identical LyC and UV morphologies suggest that the covering fraction of neutral gas and dust, the two known sources of LyC opacity, is residual or negligible. It also suggests that the UV starlight is dominated by O-type stars that emit both LyC and UV photons, which is consistent with the strong wind line profiles seen in the rest-UV spectrum (e.g. N IV λ1240, C IV λ1550; Marques-Chaves et al. 2022). Our results thus support the very high $f_{\rm esc}^{\rm LyC} \simeq 90\%$ directly measured from the optical spectroscopy analysed in Marques-Chaves et al. (2022). The non-detection of low-ionisation ISM absorption lines in the optical spectrum of J1316+2614 and its steep UV slope ($\beta_{\rm UV} \simeq -2.60$; Marques-Chaves et al. 2022) are also consistent with residual gas and dust along the line of sight (e.g. Gazagnes et al. 2018; Chisholm et al. 2022; Saldana-Lopez et al. 2022).

The left panel of Fig. 7 shows the continuum-subtracted Lyα emission obtained from HST/$FR551N$ (blue). Lyα photons are predominantly emitted around (and far from) the compact stellar emission as traced by LyC (background image) and UV (orange). This is also highlighted in its radial profile seen in the bottom-right panel of Fig. 7 where Lyα (blue) seems weak within the stellar component ($r < 0.1''$). It is worth noting that one of the most puzzling aspects of J1316+2614, as discussed in Marques-Chaves et al. (2022), is the reconciliation of its high LyC escape fraction with the large Lyα peak separation observed in its spectrum ($\Delta v \simeq 680\,{\rm km\,s^{-1}}$; top-right panel of Fig. 7). Since density-bounded H II regions leak LyC photons by $f_{\rm esc}^{\rm LyC} = e^{-\sigma_{\nu_0} N_{\rm HI}}$ where $\nu_0 = 6.3\times10^{-18}\,{\rm cm^2}$ is the ionisation cross-section, the observed $f_{\rm esc} \simeq 90\%$ in J1316+2614 implies a low column density of neutral gas of a few times $10^{16}\,{\rm cm^{-2}}$. This contrasts with the large Δv(Lyα) observed in J1316+2614 for which radiative transfer models predict $\log(N_{\rm HI}/{\rm cm^{-2}}) \gtrsim 21.5$ under standard assumptions (Verhamme et al. 2015). The high Δv observed in J1316+2614 can still be reconciled with a low column density of neutral gas of a few times $10^{16}\,{\rm cm^{-2}}$, but this requires a fairly high Doppler broadening parameter suggestive of, for example, turbulent gas (Dijkstra 2019). Whether the gas traced by Lyα is optically thick or thin but highly turbulent, this apparent discrepancy seems now solved: Lyα photons are predominantly emitted far from the LyC regions of J1316+2614, and, therefore, the high $f_{\rm esc}^{\rm LyC}$ and large Δv(Lyα) can be naturally reconciled.

Furthermore, the Lyα spectral profile analysed in Marques-Chaves et al. (2022) also reveals relatively weak emission at the systemic velocity, which should trace the closest gas around the stars. Given that a low column density of neutral gas (of approximately a few times $10^{16}\,{\rm cm^{-2}}$) is necessary for the high $f_{\rm esc}^{\rm LyC} \simeq 90\%$, the weak Ly$\alpha$ emission at the systemic velocity may suggest a low amount of ionised gas within and in front the UV stellar component, consistent with the Lyα geometry and its hole shown in Fig. 7. A substantial offset between H II regions and stars in J1316+2614 could also explain its relatively low $O32 = $ [O III] λ5008/[O II] λ3727 $= 4.8 \pm 2.1$ (Marques-Chaves et al. 2022) compared to other strong LyC emitters (e.g. Jaskot & Oey 2013; Izotov et al. 2018), and therefore its low ionisation parameter ($\propto d^{-2}$, where d is the distance between the ionised gas and stars). This should be confirmed with high-spatial-resolution observations of the nebular emission traced by non-resonant lines.

All the aforementioned points refer to the LyC, UV, and gas distributions along the line of sight, and variations of $f_{\rm esc}^{\rm LyC}$ and Lyα properties with sight-line are certainly expected (e.g. Verhamme et al. 2012; Mauerhofer et al. 2021; Blaizot et al. 2023; Gazagnes et al. 2024). However, the analysis by Marques-Chaves et al. (2022) relating the observed Hβ luminosity with the production rate of LyC photons suggests that the total ($\approx 4\pi$) LyC escape fraction in J1316+2614 is globally high ($f_{\rm esc}^{\rm LyC,4\pi} \approx 80\%$). This conclusion arises from the simple conservation of ionising photons[4] and the fact that the non-resonant Hβ emission is weakly affected by sight-line variations, in particular when dust-attenuation levels are residual (as in the case of J1316+2614).

Finally, we discuss the ALMA observations of J1316+2614 presented in Dessauges-Zavadsky et al. (in prep.). J1316+2614 was observed in Bands 3 and 6 to probe the molecular gas and dust emission, respectively. The molecular gas, traced by CO(4-3), is not detected with a 4σ velocity-integrated intensity limit of $I_{\rm CO} \leq 108\,{\rm mJy\,km\,s^{-1}}$. This places an upper limit on the molecular gas of $M_{\rm molgas} \leq 6.3\times10^9\,M_\odot$. On the other hand, dust emission is significantly detected (6.2σ), and a dust mass of $M_{\rm dust} = (3.5 \pm 1.0)\times10^7\,M_\odot$ is inferred (Dessauges-Zavadsky et al., in prep.). As discussed in that work, the origin of the dust remains unclear. It might have formed from supernovae in the UV-bright starburst region, although the derived dust mass slightly exceeds standard predictions (Gall & Hjorth 2018) even without considering dust destruction. The observed dust could also be produced before the UV-bright starburst by an older, still undetected stellar population. Despite the relatively low spatial resolution (beam size of $1.70'' \times 1.33''$), the dust emission is resolved with an effective radius of $r_{\rm eff}^{\rm dust} = 1.7 \pm 0.8$ kpc. If dust and gas are coupled, the dust distribution could follow that traced by Lyα, which might explain its relatively large size. We would expect the dust emission to also show a 'hole' or be distributed in a shell, similar to Lyα. High angular resolution observations will be needed to test this. In any case, the steep UV slope ($\beta_{\rm UV} \simeq -2.60$) and the fairly blue ($f_\nu$) SED of J1316+2614 indicate residual dust attenuation in the starlight. Thus, it is likely

[4] The Hβ luminosity should be proportional to the production rate of ionising photons, $Q_{\rm H}$, in the form $L({\rm H}\beta) \propto {\rm Q_H} \times [1 - {\rm f_{esc}^{LyC}}]$.

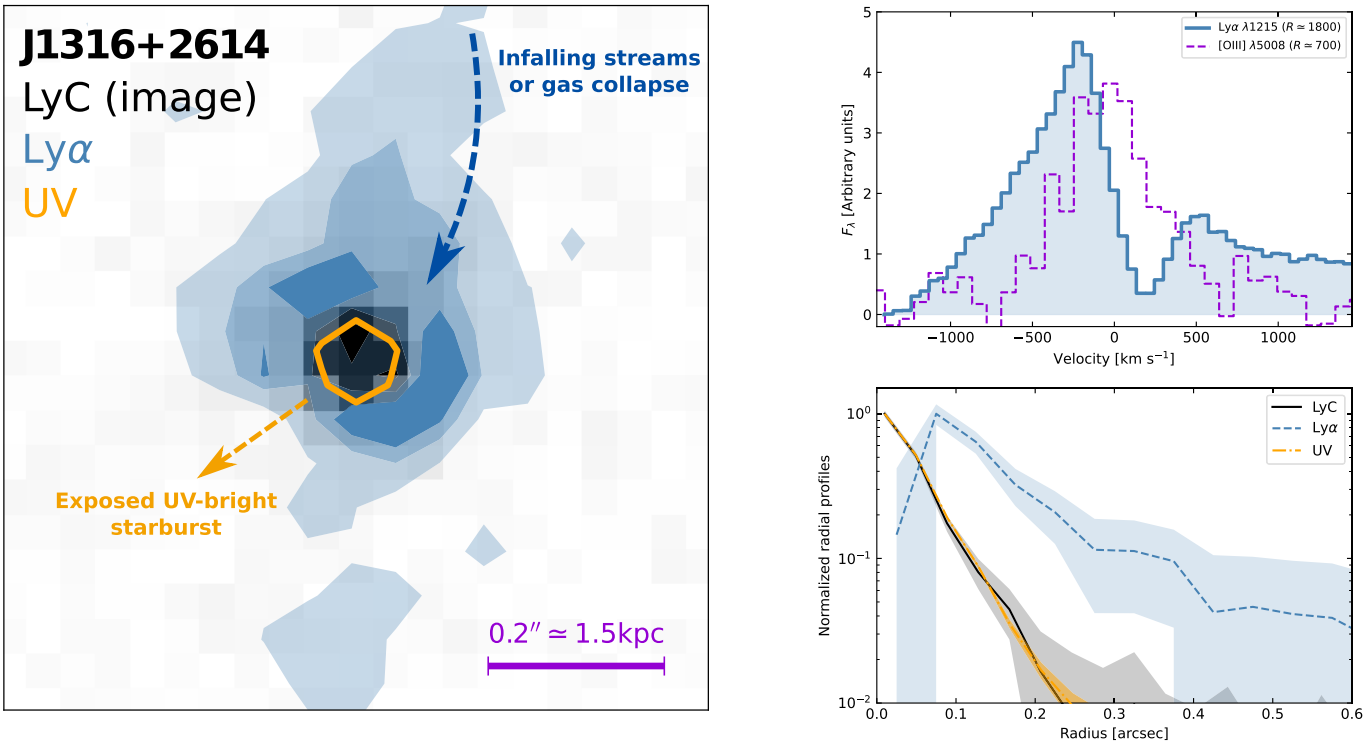

Fig. 7. LyC emission of J1316+2614 from the HST/$F410M$ image ($0.8'' \times 0.8''$; north is up, and east is to the left). The continuum-subtracted Lyα emission is shown in blue with three contours representing the $2.5\sigma - 5\sigma$, $5\sigma - 8\sigma$, and $8\sigma - 15\sigma$ levels. The emission from the non-ionising UV ($F775W$, $\lambda_0 \simeq 1650$ Å) is represented in orange and has a size corresponding to its observed FWHM ($\simeq 0.09''$). Top right: GTC optical and near-IR spectra analysed in Marques-Chaves et al. (2022), highlighting the Lyα λ1216 Å (blue) and [O III] λ5008 Å (violet) spectral profile at rest velocities. Bottom right: Normalised (to their maxima) radial profiles obtained for the LyC (black), UV (orange), and Lyα emission (blue).

that the dust and stellar emission from the UV-bright starburst are not co-spatial.

In short, the various independent observations analysed in this section all indicate that the young, UV-bright starburst in J1316+2614 is likely exposed (i.e. nearly devoid of gas and dust). While gas and dust are present around the starburst, these appear to be residual within it. Under these conditions, LyC photons are free to escape.

4.3. Energetics and the need for a high star-formation efficiency

The exposed nature of J1316+2614 raises an important question: how can such a vigorous starburst be almost devoid of gas? Although these conditions are extreme on a galaxy-wide scale, they are common in local star clusters and have been studied extensively over the past decade (e.g. Baumgardt et al. 2008; Bastian & Strader 2014; Krause et al. 2016). The basic principle is that feedback from mechanical and radiative outflows must surpass the gravitational binding force, ejecting the remaining gas from star-forming clouds and leaving an exposed stellar component. In the following, we investigate the different energetic processes associated with J1316+2614.

We assumed the Plummer star cluster model, in which the gravitational binding energy of the gas is given by $E_\mathrm{b} = k(1 - \epsilon_\mathrm{SF})GM_\mathrm{T}^2/r_h$ (Baumgardt et al. 2008). Here, k is a dimensionless constant ($\approx$0.4), ϵ_SF is the star-formation efficiency, and M_T is the total mass enclosed within the half-mass radius r_h (where $r_\mathrm{h} \simeq 1.7 \times r_\mathrm{eff}$ in a Plummer sphere). The factor $(1-\epsilon_\mathrm{SF})$ accounts for the fact that a fraction of the gas is converted into stars. We estimated E_b as a function of ϵ_SF assuming that $M_\mathrm{T} \simeq M_\star + M_\mathrm{gas}$ and $\epsilon_\mathrm{SF} = M_\star/M_\mathrm{T}$. The left panel of Fig. 8 shows the binding energies for J1316+2614 obtained with ϵ_SF of 0.4, 0.7, and 0.95 (horizontal red lines). For simplicity, we assumed that E_b remains constant over time.

We also examined the mechanical energy from stellar winds and supernovae as a function of age. Predictions for the kinematic energy of J1316+2614 were obtained from BPASS v2.2.1 models (Stanway & Eldridge 2018), assuming a constant star formation of SFR = 898 $M_\odot\,\mathrm{yr}^{-1}$, a metallicity of $Z = 0.008$ and the Chabrier (2003) IMF, reflecting the properties of the young starburst derived in Sect. 3.3. The outputs of the wind and supernova energy of J1316+2614 are shown in the left panel of Fig. 8 in green and yellow, respectively. As shown, the total mechanical energy (winds and supernovae) surpasses the binding energy feedback only if the star-formation efficiency in J1316+2614 is $\epsilon_\mathrm{SF} \geq 0.7$ (at the age of J1316+2614). In other words, gas expulsion from stellar winds and supernovae can only occur if $\epsilon_\mathrm{SF} \geq 0.7$. Before the onset of supernova feedback ($\lesssim$3.5 Myr), stellar winds appear relatively inefficient in removing the gas, requiring star-formation efficiencies as high as $\epsilon_\mathrm{SF} \gtrsim 0.95$.

Given that binding energy is proportional to M^2/r and the mechanical energy proportional to M, Krause et al. (2016) introduced the compactness index $C_5 = M_\odot/r_h$. This index relates the critical star-formation efficiency, above which the kinetic energy surpasses the gravitational binding, leading to gas expulsion. The right panel of Fig. 8 shows the C_5 derived for J1316+2614, $C_5 = 128 \pm 11$ ($10^5\,M_\odot\,\mathrm{pc}^{-1}$), along with the critical star-formation efficiency needed for gas expulsion by stellar winds (green), supernovae (yellow, $E_0 = 10^{51}$ erg) and hypernovae (red, $E_0 = 10^{53}$ erg) derived in Krause et al. (2016). Overall, the C_5 derived for J1316+2614 is much higher than typical

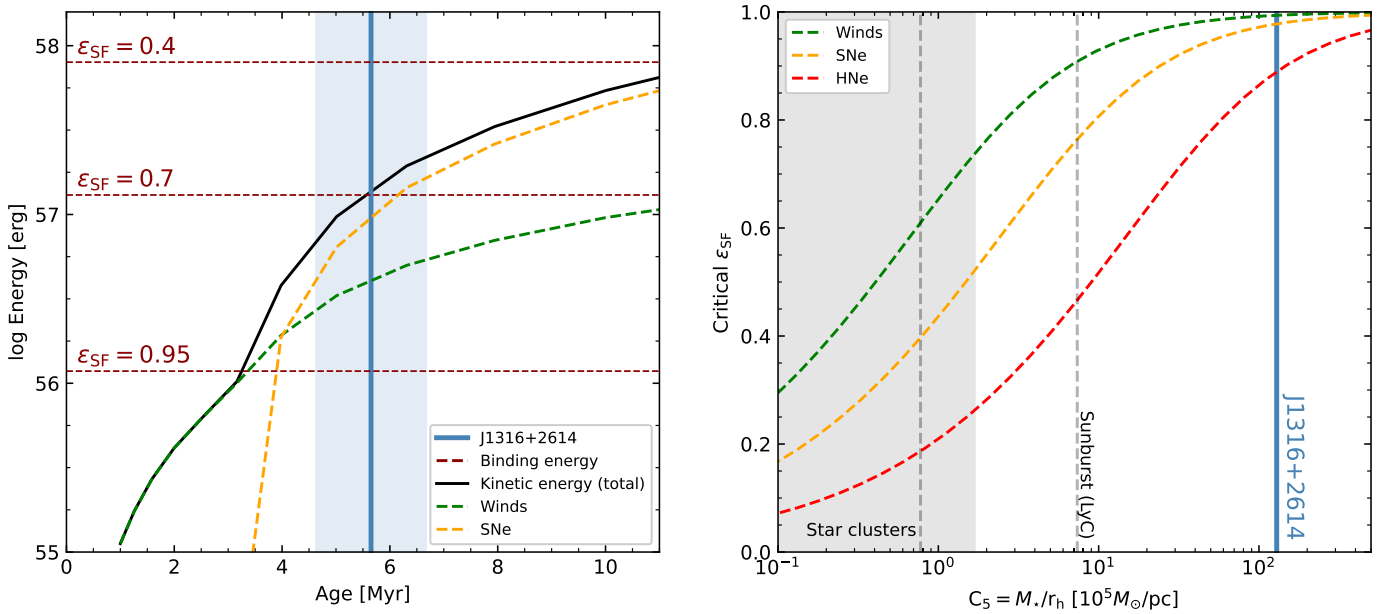

Fig. 8. Inferred energetics for J1316+2614. Left: Different energies associated with J1316+2614. Binding energies are shown in dark red (horizontal dashed lines) for star-formation efficiencies of 0.4, 0.7, and 0.95. The total kinetic energy is shown in black and includes the contribution of stellar winds (dashed green line) and supernovae (dashed yellow line). They are obtained from BPASS models assuming a continuous star-formation history with SFR = 898 $M_\odot$ yr^{-1}, Z = 0.008 and the Chabrier (2003) IMF. The age of J1316+2614 and the corresponding uncertainty are marked in blue. Right: Critical star-formation efficiency for gas expulsion by stellar winds (green), normal supernovae (10^{51} erg, yellow), and hypernovae (10^{53} erg, red) as a function of the compactness index C_5 as proposed by Krause et al. (2016). The location of J1316+2614 is shown in blue. The compactness indexes of other star clusters, including the Sunburst cluster, are marked with dashed grey lines.

values in star clusters ($C_5 \lesssim 1$; Krause et al. 2016), implying also a much higher ϵ_{SF} to remove the gas within the stellar core of J1316+2614. However, we note that the critical star-formation efficiencies shown in this figure were calibrated for star clusters (i.e. assuming a single age burst; Krause et al. 2016). Whether J1316+2614 can be described as a single burst is still unclear (see Sect. 4.1).

We also explored the effects of radiative-driven outflows, which were recently proposed to explain the overabundance of UV-bright galaxies at high redshifts (Ferrara et al. 2023). Following Ziparo et al. (2023), we determined the conditions under which radiation pressure can drive an outflow by comparing the Eddington ratio as a function of ΣSFR. Considering ΣSFR $\simeq 3\times10^3\ M_\odot\ \mathrm{yr}^{-1}\ \mathrm{kpc}^{-2}$ derived for J1316+2614, a radiative-driven outflow can occur when the burstiness parameter is $k_s \gtrsim 56$, which quantifies the deviation from the Kennicutt-Schmidt relation (i.e. $\Sigma\mathrm{SFR} \propto k_s \Sigma_{gas}^{1.4}$). This translates to an upper limit of the gas surface density of $\Sigma_{gas} \lesssim 6\times10^3 M_\odot\ \mathrm{pc}^{-2}$. Assuming gas and stars had the same size, we find that $\epsilon_{SF} \gtrsim 0.72$ is needed to launch radiation-driven outflows efficiently. This is consistent with recent radiation hydrodynamic simulations of the formation of massive star clusters, where clusters with $\Sigma M \simeq 10^3$–$10^5\ M_\odot\ \mathrm{pc}^{-2}$ became super-Eddington when high star-formation efficiencies are reached ($\epsilon_{SF} \sim 80\%$; Menon et al. 2023).

Our results thus support a very high star-formation efficiency in J1316+2614. The exposed, gas-free nature of the UV-bright starburst in J1316+2614 suggests that either all the gas was converted into stars ($\epsilon_{SF} \sim 1$) or it was partially ejected by mechanical or radiative feedback, which still requires a fairly high $\epsilon_{SF} \gtrsim 0.7$. Feedback seems indeed ineffective in J1316+2614 to suppress star formation, as seen from the inflowing signatures suggested from its Lyα profile. This inefficient feedback could enhance the star-formation efficiency and SFR of J1316+2614, explaining also its remarkably high UV luminosity (e.g. Renzini 2023). The high star-formation efficiency is also corroborated by the non-detection of molecular gas using ALMA ($M_{gas} \leq 6.3\times10^9\ M_\odot$), for which an $\epsilon_{SF} \geq 0.4$ was derived (Dessauges-Zavadsky et al., in prep.). On the other hand, we acknowledge that these analytic expressions are likely too simple to explain the complex ISM conditions and kinematics of J1316+2614, not considering, for example, possible effects of hot X-ray-emitting gas, turbulence, the multi-phase nature of the ISM, or even the presence of an active galactic nucleus (see e.g. Krause et al. 2020; Thompson & Heckman 2024, and references therein), although there are currently no signs of such phenomena in our target (Marques-Chaves et al. 2022). Additionally, the energies and ϵ_{SF} considered here also depend on the stellar mass derived for J1316+2614, which is sensitive to the adopted IMF (e.g. Menon et al. 2024a). In this context, VMSs have been suggested in J1316+2614 (and in other similar UV-bright galaxies; Upadhyaya et al. 2024) from its intense and broad He II λ1640 emission (e.g. Martins & Palacios 2022; Martins et al. 2023). However, they appear to provide only modest changes on the UV mass-to-light ratio, decreasing it by ≈×1.5 (Schaerer et al. 2024b).

4.4. High star-formation efficiency and high LyC escape: Cause and effect

Several surveys have been conducted to understand the conditions under which LyC photons can escape from star-forming galaxies (e.g. Steidel et al. 2018; Flury et al. 2022). The standard paradigm assumes that LyC leakage occurs through ionised channels in the ISM originated by strong feedback mechanisms (e.g. Heckman et al. 2001). Observations do suggest the importance of mechanical and radiative driven winds in the escape of LyC photons (e.g. Komarova et al. 2021; Bait et al. 2024; Amorín et al. 2024; Carr et al. 2024).

In the case of J1316+2614, mechanical and radiative feedback alone seems insufficient to clear the gas within the starburst, at least from a simple energetic balance. As highlighted before, gas clearance from mechanical and radiative feedback requires a fairly high star-formation efficiency. Regardless of the presence of strong feedback, an $\epsilon_{\rm SF} \gtrsim 0.7$ is necessary to account for the exposed nature of J1316+2614 and its resulting high LyC leakage. If instead J1316+2614 had a more typical star-formation efficiency (e.g. $\lesssim$0.1), it would likely contain large amounts of gas ($M_{\rm gas} \gtrsim 4 \times 10^{10}\,M_\odot$), increasing considerably the gravitational binding energy ($E_{\rm b} \gtrsim 10^{59}$ erg). Under these conditions, the kinetic energy ($E_{\rm kin} \simeq 10^{57}$ erg; Fig. 8) would be insufficient to expel the gas from the stellar core, likely preventing LyC leakage. Our results thus support that, although mechanical and radiative outflows may be significant in J1316+2614 (though not detected so far), the high star-formation efficiency seems to be the primary driver for the high LyC escape in J1316+2614.

A causal relationship between high star-formation efficiencies and increased LyC production and leakage is expected (see Jecmen & Oey 2023; Kimm et al. 2019; Menon et al. 2024b). Simply put, higher $\epsilon_{\rm SF}$ within a star-forming region inevitably results in less residual gas to absorb LyC photons. Additionally, this remaining gas would be more easily removed from the starburst region, as higher $\epsilon_{\rm SF}$ enhances both mechanical and radiative energies (both proportional to SFR or $M_\star$, i.e. $\propto \epsilon_{\rm SF} M_{\rm T}$), and decreases the binding energy ($\propto (1-\epsilon_{\rm SF}) M_{\rm T}^2$). Moreover, an increased $\epsilon_{\rm SF}$ would boost the SFR, leading to the formation of more massive stars and thereby increasing LyC emission. This could also lead to density-bounded regions, which facilitates LyC escape (e.g. Jaskot et al. 2017). Hence, the impact of high $\epsilon_{\rm SF}$ on LyC escape is twofold: it not only enhances the production of ionising photons but also facilitates their escape.

While J1316+2614 may represent an extreme case with LyC leakage possibly enhanced by its high star-formation efficiency, similar conditions might be already present in other cases. For example, the well-studied, gravitationally lensed Sunburst cluster at $z = 2.37$ is known to leak large amounts of LyC photons (Dahle et al. 2016; Rivera-Thorsen et al. 2017, 2019; Vanzella et al. 2020). Meštrić et al. (2023) show that the LyC region is slightly smaller ($r_{\rm eff}^{\rm LyC} \simeq 5$ pc) than the non-ionising region ($r_{\rm eff}^{\rm UV} \simeq 8$ pc), suggesting that the Sunburst cluster is, at least, partially exposed[5]. Using the stellar mass derived in Vanzella et al. (2022) of $10^7\,M_\odot$ and the half-mass radius of $r_{\rm h} \simeq 1.7 \times r_{\rm eff}^{\rm UV}$, the Sunburst cluster shows a high compactness index of $C_5 \simeq 7.5$ ($10^5\,M_\odot\,{\rm pc}^{-1}$), which is a factor of $\approx\times$10 higher than in local star clusters (e.g. Bastian & Strader 2014; Krause et al. 2016). If the outflows detected by Mainali et al. (2022) and Vanzella et al. (2022) are responsible for the gas clearance in the Sunburst cluster, then its high C_5 suggests a high $\epsilon_{\rm SF}$, at least $\gtrsim$0.45 as seen in the right panel of Fig. 8.

In short, our results suggest a close relationship between high $\epsilon_{\rm SF}$ and high escape of ionising photons. This may be particularly relevant at higher redshifts, where star-formation efficiencies are expected to be higher due to the higher densities and lower metallicities of the ISM in high-z galaxies (e.g. Dekel et al. 2023; Ceverino et al. 2024). Thus, high star-formation efficiencies could not only be crucial for the mass growth of high-z galaxies (e.g. Xiao et al. 2023; de Graaff et al. 2024; Glazebrook et al. 2024; Weibel et al. 2024), but may also have important implications for cosmic re-ionisation.

[5] It can still be fully exposed if the LyC emitting stars are segregated in the centre of the cluster (see the discussion in Meštrić et al. 2023).

4.5. Feedback-free starburst within an extreme formation mode

4.5.1. J1316+2614 as an intense feedback-free starburst?

The high star-formation efficiency in J1316+2614 likely plays a key role in enhancing its SFR and burst mass. In this context, high star-formation efficiencies have been recently proposed to explain the high-number density of UV-bright and massive sources at early times (Dekel et al. 2023; Li et al. 2024; Ceverino et al. 2024). Following Dekel et al. (2023), high-density environments and low metallicities could favour the formation of FFBs (Dekel et al. 2023) through the collapse of gas clouds within very short free-fall times. This would promote higher star-formation efficiencies, as the cloud collapse occurs before the onset of mechanical feedback. High-mass galaxies could thus form quickly through several generations of FFBs.

The very high mass density of J1316+2614 indeed suggests a rather short free-fall time. Assuming a spherical gas geometry with a radius of $r_{\rm eff}$, and a star-formation efficiency of 0.7, we derive the free-fall time $t_{\rm ff} \simeq 1.1$ Myr, where $t_{\rm ff} = \sqrt{3\pi/(32\,G\,\rho)}$ and $\rho = 3\,M_{\rm gas}/(4\pi\,r_{\rm eff}^3)$. Therefore, the derived free-fall time in J1316+2614 is within the range predicted by the FFB scenario ($\sim$1 Myr; Dekel et al. 2023). Additionally, J1316+2614 shows a very compact morphology ($r_{\rm eff} \simeq 220$ pc), which aligns with predictions for galaxies in the FFB phase ($r_{\rm eff} \sim 300$ pc) as discussed in Li et al. (2024).

On the other hand, the metallicity inferred for J1316+2614 using the $R23$ method ($12+\log({\rm O/H}) = 8.45 \pm 0.12$; Marques-Chaves et al. 2022) is higher than expected in the FFB scenario ($\sim$0.1 $Z_\odot$; Dekel et al. 2023). However, the derived O/H abundance should also reflect the likely efficient chemical enrichment of the starburst itself over the last 5–6 Myr, potentially differing from the gas metallicity in the pre-FFB phase. Furthermore, the derived abundance in J1316+2614 should be treated with caution due to the underlying effect of high $f_{\rm esc}^{\rm LyC}$, as discussed by Marques-Chaves et al. (2022). We also compared the star-formation history of J1316+2614 with those expected in an FFB galaxy (Li et al. 2024). Using the derived SFR $= 898\,M_\odot\,{\rm yr}^{-1}$ and the upper limit on the molecular mass $M_{\rm molgas} \leq 6.3 \times 10^9\,M_\odot$, the gas depletion timescale is $t_{\rm depl} = M_{\rm molgas}/{\rm SFR} \lesssim 7$ Myr. Considering its age, the duration of the UV-bright starburst in J1316+2614 should be around $\Delta t \simeq 6-13$ Myr. The star-formation history of J1316+2614 appears slightly different (higher SFR and higher Δt) than the predictions by Li et al. (2024, see their Sect. 4).

In short, being among the most powerful starbursts known and showing no evidence of feedback so far, J1316+2614 may represent a case of an intense FFB with high star-formation efficiency. This would support the link between high star-formation efficiencies and high UV-luminosities, as suggested for galaxies at very high redshifts (Dekel et al. 2023; Li et al. 2024).

4.5.2. Very efficient stellar mass growth

We further investigated the impact of this extreme UV-bright starburst on the stellar mass growth of J1316+2614. Our multi-wavelength SED analysis in Sect. 3.3 indicates that the young starburst dominates the light (UV-optical) and likely the mass of J1316+2614. Even with conservative assumptions for the old stellar population (1.4 Gyr old), our best-fit CIGALE model predicts a relatively faint stellar component with $\log(M_\star^{\rm old}/M_\odot) \leq 9.46$ (3σ). If so, it could also explain the origin of the dust observed in J1316+2614 ($M_{\rm dust} = 3.5 \times$

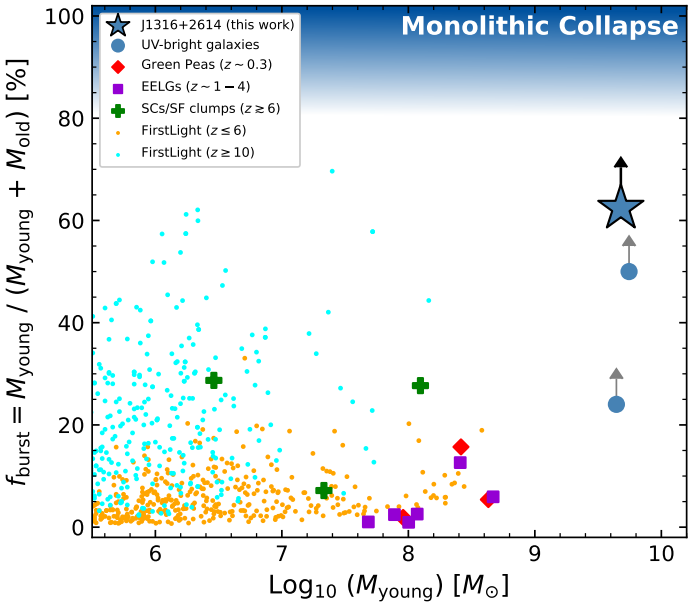

Fig. 9. Contribution (as a percentage) of the starburst mass (≤10 Myr) to the total mass of J1316+2614 (blue star) and other star-bursting galaxies, including UV-bright galaxies at $z \simeq 2-3$ (blue circles; Marques-Chaves et al. 2020a, 2021), extreme [O III] λ5008 emitters at $z \sim 1-4$ (violet squares; Tang et al. 2022), and local Green Pea galaxies (red diamonds; Amorín et al. 2012). Green crosses mark the measurements of highly magnified galaxies at $z \gtrsim 6$ for which young star clusters or star-forming regions are resolved (Vanzella et al. 2023; Adamo et al. 2024; Fujimoto et al. 2024). FirstLight-simulated sources at $z \simeq 5-6$ and $z \gtrsim 10$ are also shown as orange and cyan dots, respectively (Ceverino et al. 2017).

$10^7\,M_\odot$, Dessauges-Zavadsky et al., in prep.). Following the $M_{\rm dust} - M_\star$ relation derived by Magnelli et al. (2020), we would expect a stellar mass of the underlying old stellar population of $\log(M_\star^{\rm old}/M_\odot) \simeq 9.2$, which would be consistent with our upper limit. Assuming $\log(M_\star^{\rm old}/M_\odot) \leq 9.46$, the UV-bright starburst accounts for a large fraction of the stellar mass of J1316+2614, $f_{\rm burst} = M_\star^{\rm young}/(M_\star^{\rm young} + M_\star^{\rm old}) \geq 62\%$ (3σ).

Figure 9 shows the $f_{\rm burst}$ derived for J1316+2614 (blue star). We also show measurements obtained for other galaxies, including other similar UV-bright galaxies, extreme [O III] λ5008 emitters at $z \sim 1-4$, and local Green Pea galaxies.

Green Pea and extreme [O III] emitters are vigorous star-bursting galaxies, but their young (≲10 Myr) stellar populations account for a relatively small fraction of the total mass (with a mean a standard deviation of $f_{\rm burst} = 6 \pm 5\%$). This figure also shows the $f_{\rm burst}$ derived for two other UV-bright galaxies, J1220+0842 ($f_{\rm burst} \geq 50\%$; Marques-Chaves et al. 2020a) and J0146-0220 ($f_{\rm burst} \geq 24\%$; Marques-Chaves et al. 2021), whose properties closely resemble those of J1316+2614 (e.g. $M_{\rm UV} < -24$). Interestingly, Dessauges-Zavadsky et al. (in prep.) find high star-formation efficiencies for these two sources, up to $\epsilon_{\rm SF} \geq 24\%$. For more normal, main-sequence galaxies, the $f_{\rm burst}$ parameter is likely even smaller. This is highlighted in Fig. 9 where we show the predictions from FirstLight simulations (Ceverino et al. 2017). Simulated sources at $z \simeq 5-6$ (orange dots) show relatively modest $f_{\rm burst} \simeq 5\%$ on average. At higher redshifts, FirstLight-simulated sources at $z \gtrsim 10$ (cyan dots) show higher stellar mass growth efficiencies, with $f_{\rm burst} \simeq 15\%$ on average, likely due to the burstier nature of high-z sources and the limited time to form evolved stellar populations. Star-forming clumps at $z \sim 6-10$ recently observed in lensed galaxies seem indeed to contribute substantially to the total mass of these early galaxies, up to $f_{\rm burst} \simeq 30\%$ (green in Fig. 9; Vanzella et al. 2023; Adamo et al. 2024; Fujimoto et al. 2024).

If the star-formation efficiency in J1316+2614 is effectively high, our results suggest that it can have a huge impact on the stellar mass growth in the galaxy. Indeed, the high stellar mass fraction formed in the starburst in J1316+2614 ($f_{\rm burst} \geq 62\%$) resembles traditional models of monolithic collapse, where most of its mass is assembled within a remarkably short period of time (e.g. Eggen et al. 1962; Larson 1976; Matteucci 1994).

4.6. Possible formation paths

How can J1316+2614 be so UV-bright, compact, massive, and young? Here, we explore possible formation paths for this extreme starburst. Extended Lyα halos, like the one seen in J1316+2614, are commonly observed around high redshift star-forming galaxies (e.g. Leclercq et al. 2017; Kusakabe et al. 2022). However, signatures of inflowing gas indicated by blue-dominated Lyα profiles are extremely rare (e.g. Erb et al. 2014; Martin et al. 2015). Typically, star-forming galaxies show Lyα profiles dominated by redshifted emission along with blueshifted ISM absorption lines, both consistent with large-scale outflows (e.g. Shapley et al. 2003; Steidel et al. 2010; Leclercq et al. 2020; Marques-Chaves et al. 2020b). Therefore, it is tempting to associate the extreme nature of J1316+2614 with the inflowing gas suggested by its Lyα profile (see the discussion in Marques-Chaves et al. 2022).

The rapid mass assembly history of J1316+2614, forming $\simeq 5 \times 10^9\,M_\odot$ of stars in just ≃5−6 Myr, along with its compactness and the absence of a significant old stellar population, suggests an extreme formation path, potentially monolithic. Inflowing streams or massive gas collapse could trigger and feed the young starburst in J1316+2614. This could provide enough gas supply for a globally high star-formation efficiency (e.g. as required for the FFB; Dekel et al. 2023). Thus, the filamentary-like gas distribution traced by Lyα emission (see Fig. 7) could represent remnants of the infalling streams, supporting its Lyα spectral profile (e.g. Dijkstra et al. 2006). However, the real extent of this inflowing gas and whether it consists of pristine or recycled material from previous star-formation episodes (e.g. galactic fountains) remains unknown.

Alternatively, the inflowing gas kinematics could be related to dissipative compaction of the gas disc induced by a wet merger or by violent disc instabilities (e.g. Zolotov et al. 2015), as discussed in Marques-Chaves et al. (2022). However, simulations of the compaction phase predict a modest increase in the sSFR with respect to the main sequence, of $\Delta\log(\mathrm{sSFR}) \simeq 0.3-0.7$ dex (Zolotov et al. 2015; Tacchella et al. 2016), while J1316+2614 shows $\Delta\log(\mathrm{sSFR}) \simeq 1.7$ dex (assuming $\mathrm{sSFR} = 188 \pm 40\,\mathrm{Gyr}^{-1}$). Furthermore, the (stellar) disc remains undetected in our deep, high-resolution images. Finally, typical major merger processes involve timescales that are likely too long to explain the observed properties of J1316+2614 (e.g. Lotz et al. 2008). Given the very young age of J1316+2614, we would expect to observe multiple merging clumps or galaxies. However, HST images reveal only a very compact stellar morphology with a half-light radius of ≃220 pc. The Lyα emission shows a complex, filamentary-like morphology (oriented south to north; Figs. 4 and 8), which could, in principle, represent tidal tails from merging galaxies. However, such a configuration is unlikely given the short timescales involved in J1316+2614 (≃6 Myr). Moreover, merging galaxies would likely present

evolved stellar populations, but these have not been detected so far in J1316+2614. Therefore, a typical major merger seems unlikely to be the direct cause of this intense starburst, though a rare merging configuration cannot be ruled out.

5. Summary and conclusions

In this paper we have presented high-resolution HST and VLT imaging observations of J1316+2614, which was discovered by Marques-Chaves et al. (2022) at $z = 3.613$. J1316+2614 is so far the UV-brightest ($M_{\rm UV} = -24.7$) star-forming galaxy known and one of the strongest LyC emitters, with an escape fraction of $f_{\rm esc}^{\rm LyC} \approx 90\%$. It also shows a steep UV slope ($\beta_{\rm UV} \simeq -2.60$) and a peculiar, blue-dominated Lyα emission, which indicates inflowing gas. The new HST observations probe the LyC, Lyα, rest-UV, and optical emission of J1316+2614 with WFC3/$F410M$, ACS/$FR551N$, WFC3/$F775W$, and WFC3/$F160W$, respectively. Seeing-enhanced $K_{\rm s}$-band observations were obtained with VLT/HAWK-I (FWHM $\simeq 0.30''$). From the analysis of these data, we arrived at the following main conclusions:

- J1316+2614 shows a very compact but resolved morphology in the LyC and rest-UV. Using `PySersic` we find similar half-light radii for the LyC and UV emission of $r_{\rm eff}^{\rm LyC} = 262 \pm 64$ pc and $r_{\rm eff}^{\rm UV} = 220 \pm 12$ pc, respectively. J1316+2614 represents the first known case of resolved LyC emission in a star-forming galaxy. The LyC and UV radial profiles and residuals obtained from the PSF-subtracted images are also indistinguishable within the uncertainties. Our results suggest that the LyC and UV morphologies and sizes are essentially the same ($r_{\rm eff} \simeq 220$ pc), indicating a residual covering fraction of neutral gas and very high LyC leakage. On the other hand, J1316+2614 appears unresolved at longer wavelengths in HST/$F160W$ and VLT/$K_{\rm s}$ images ($r_{\rm eff}^{\rm opt} \leq 440$ pc).
- The HST ACS/$FR551N$ ramp-filter image ($\lambda_{\rm eff} \simeq 5604$ Å and width of $\simeq$97 Å), which traces the Lyα emission of J1316+2614, shows a well-resolved morphology with a filamentary-like emission with a total scale length of $\simeq$6.0 kpc (3σ) oriented south to north. After subtracting the contribution of the underlying stellar continuum, Lyα appears residual at the position of the stellar (LyC and UV) emission. Our results indicate a Lyα hole with weak Lyα emission co-spatial with the stellar continuum. This configuration, combined with the steep UV slope, lack of ISM absorption lines, similar LyC and UV morphologies, and high LyC escape fraction, suggests that gas and dust are residual within the starburst (though present around it).
- Using the photometry obtained from the new images, we re-analysed J1316+2614's SED. We find that J1316+2614 is dominated by an almost un-obscured ($E(B-V) = 0.03 \pm 0.01$) young stellar population with an age of 5.7 ± 1.0 Myr and a continuous SFR $= 898 \pm 181\, M_\odot\,{\rm yr}^{-1}$. The mass formed in this young starburst is $M_\star^{\rm young} = (4.8 \pm 0.3) \times 10^9\, M_\odot$. The SFR and stellar mass surface densities, $\log(\Sigma SFR[M_\odot\,{\rm yr}^{-1}\,{\rm kpc}^{-2}]) = 3.47 \pm 0.11$ and $\log(\Sigma M_\star[M_\odot\,{\rm pc}^{-2}]) = 4.20 \pm 0.06$, are among the highest found in star-forming galaxies, resembling those observed in local young massive star clusters.
- We also investigated the possible presence of an underlying old stellar population, which is not detected. Assuming a 1.4 Gyr old burst model, we place an upper limit on its mass of $M_\star^{\rm old} \leq 2.8 \times 10^9\, M_\odot$ (3σ). Our results suggest that the UV-bright starburst dominates not only the light emission of J1316+2614 (≃100%) but also its stellar mass, with a mass fraction of the galaxy formed in the last ≃6 Myr of $f_{\rm burst} = M_\star^{\rm young}/(M_\star^{\rm young} + M_\star^{\rm old}) \geq 62\%$ (3σ). Our results suggest that the bulk of the stellar mass in J1316+2614 was assembled within a remarkably short period of time, resembling models of monolithic collapse.

The emerging picture of J1316+2614 consists of a very powerful, young, and compact starburst leaking a significant fraction of LyC photons due to a lack of gas and dust within its stellar core. Using simple analytic expressions and assumptions, we explored the different energetic processes associated with J1316+2614 and the conditions leading to its exposed nature. Feedback seems ineffective in J1316+2614 under normal conditions, and a very high star-formation efficiency ($\epsilon_{\rm SF} \geq 0.7$) is expected to expel the remaining gas from the starburst region. Thus, our results support the notion that, although mechanical and radiative outflows may be present in J1316+2614 (though not detected so far), the high star-formation efficiency is likely the main driver for the high LyC escape in J1316+2614.

Overall, the high star-formation efficiency in J1316+2614 provides a natural explanation for its remarkably high $f_{\rm esc}^{\rm LyC}$, SFR, and UV luminosity, as well as the lack of molecular gas ($M_{\rm molgas} \leq 6.3 \times 10^9\, M_\odot$; Dessauges-Zavadsky et al, in prep.). It also explains the very efficient stellar mass growth in J1316+2614, with at least 62% of its mass formed in the last 6 Myr. In this context, J1316+2614 may be an intense FFB with a high star-formation efficiency, similar to those proposed for UV-bright galaxies at very high redshifts. If similar conditions are present in their higher-z counterparts, our results suggest that high star-formation efficiencies could be crucial not only for the accelerated mass buildup of high-z galaxies but also for promoting LyC production and escape, with possible implications for cosmic re-ionisation.

Acknowledgements. The authors thank the referee for useful comments. We would like to thank Angela Adamo and Adélaïde Claeyssens for sharing the data presented in Fig. 6. This research is based on observations made with the NASA/ESA *Hubble* Space Telescope obtained from the Space Telescope Science Institute, which is operated by the Association of Universities for Research in Astronomy, Inc., under NASA contract NAS 5–26555. These observations are associated with programme 17286. Based on observations collected at the European Southern Observatory under ESO programme 111.251K.001. J.A-M. and L.C. acknowledge support by grant PIB2021-127718NB-100 from the Spanish Ministry of Science and Innovation/State Agency of Research MCIN/AEI/10.13039/501100011033 and by "ERDF A way of making Europe".

References

Adamo, A., Bradley, L. D., Vanzella, E., et al. 2024, Nature, 632, 513
Álvarez-Márquez, J., Marques-Chaves, R., Colina, L., & Pérez-Fournon, I. 2021, A&A, 647, A133
Amorín, R., Pérez-Montero, E., Vílchez, J. M., & Papaderos, P. 2012, ApJ, 749, 185
Amorín, R. O., Rodríguez-Henríquez, M., Fernández, V., et al. 2024, A&A, 682, L25
Arrabal Haro, P., Dickinson, M., Finkelstein, S. L., et al. 2023, ApJ, 951, L22
Bait, O., Borthakur, S., Schaerer, D., et al. 2024, A&A, 688, A198
Barro, G., Faber, S. M., Koo, D. C., et al. 2017, ApJ, 840, 47
Bastian, N., & Strader, J. 2014, MNRAS, 443, 3594
Baumgardt, H., Kroupa, P., & Parmentier, G. 2008, MNRAS, 384, 1231
Bertin, E. 2006, ASP Conf. Ser., 351, 112
Birrer, S., Shajib, A., Gilman, D., et al. 2021, J. Open Source Softw., 6, 3283
Birrer, S., Bhamre, V., Nierenberg, A., Yang, L., & Van de Vyvere, L. 2022, Astrophysics Source Code Library [record ascl:2210.005]
Blaizot, J., Garel, T., Verhamme, A., et al. 2023, MNRAS, 523, 3749
Boquien, M., Burgarella, D., Roehlly, Y., et al. 2019, A&A, 622, A103
Bouwens, R. J., Oesch, P. A., Stefanon, M., et al. 2021, AJ, 162, 47
Boylan-Kolchin, M. 2024, MNRAS, submitted [arXiv:2407.10900]

Bruzual, G., & Charlot, S. 2003, MNRAS, 344, 1000
Bunker, A. J., Saxena, A., Cameron, A. J., et al. 2023, A&A, 677, A88
Burgarella, D., Buat, V., & Iglesias-Páramo, J. 2005, MNRAS, 360, 1413
Calzetti, D., Armus, L., Bohlin, R. C., et al. 2000, ApJ, 533, 682
Carniani, S., Hainline, K., D'Eugenio, F., et al. 2024, Nature, 633, 318
Carr, C. A., Cen, R., Scarlata, C., et al. 2024, arXiv e-prints [arXiv:2409.05180]
Castellano, M., Napolitano, L., Fontana, A., et al. 2024, ApJ, 972, 143
Ceverino, D., Glover, S. C. O., & Klessen, R. S. 2017, MNRAS, 470, 2791
Ceverino, D., Nakazato, Y., Yoshida, N., Klessen, R., & Glover, S. 2024, A&A, 689, A244
Chabrier, G. 2003, ApJ, 586, L133
Charbonnel, C., Schaerer, D., Prantzos, N., et al. 2023, A&A, 673, L7
Chisholm, J., Saldana-Lopez, A., Flury, S., et al. 2022, MNRAS, 517, 5104
Claeyssens, A., Adamo, A., Richard, J., et al. 2023, MNRAS, 520, 2180
Dahle, H., Aghanim, N., Guennou, L., et al. 2016, A&A, 590, L4
de Graaff, A., Setton, D. J., Brammer, G., et al. 2024, arXiv e-prints [arXiv:2404.05683]
Dekel, A., Sarkar, K. C., Birnboim, Y., Mandelker, N., & Li, Z. 2023, MNRAS, 523, 3201
Dijkstra, M. 2019, Saas-Fee Advanced Course, 46, 1
Dijkstra, M., Haiman, Z., & Spaans, M. 2006, ApJ, 649, 14
Eggen, O. J., Lynden-Bell, D., & Sandage, A. R. 1962, ApJ, 136, 748
Erb, D. K., Steidel, C. C., Trainor, R. F., et al. 2014, ApJ, 795, 33
Ferrara, A., Pallottini, A., & Dayal, P. 2023, MNRAS, 522, 3986
Finkelstein, S. L., Bagley, M. B., Ferguson, H. C., et al. 2023, ApJ, 946, L13
Flury, S. R., Jaskot, A. E., Ferguson, H. C., et al. 2022, ApJ, 930, 126
Fruchter, A. S., & Hook, R. N. 2002, PASP, 114, 144
Fujimoto, S., Ouchi, M., Kohno, K., et al. 2024, arXiv e-prints [arXiv:2402.18543]
Gaia Collaboration (Vallenari, A., et al.) 2023, A&A, 674, A1
Gall, C., & Hjorth, J. 2018, ApJ, 868, 62
Gazagnes, S., Chisholm, J., Schaerer, D., et al. 2018, A&A, 616, A29
Gazagnes, S., Cullen, F., Mauerhofer, V., et al. 2024, ApJ, 969, 50
Glazebrook, K., Nanayakkara, T., Schreiber, C., et al. 2024, Nature, 628, 277
Heckman, T. M., Sembach, K. R., Meurer, G. R., et al. 2001, ApJ, 558, 56
Hegde, S., Wyatt, M. M., & Furlanetto, S. R. 2024, JCAP, 2024, 025
Inayoshi, K., Harikane, Y., Inoue, A. K., Li, W., & Ho, L. C. 2022, ApJ, 938, L10
Izotov, Y. I., Worseck, G., Schaerer, D., et al. 2018, MNRAS, 478, 4851
Jaskot, A. E., & Oey, M. S. 2013, ApJ, 766, 91
Jaskot, A. E., Oey, M. S., Scarlata, C., & Dowd, T. 2017, ApJ, 851, L9
Jecmen, M. C., & Oey, M. S. 2023, ApJ, 958, 149
Kannan, R., Springel, V., Hernquist, L., et al. 2023, MNRAS, 524, 2594
Kimm, T., Blaizot, J., Garel, T., et al. 2019, MNRAS, 486, 2215
Komarova, L., Oey, M. S., Krumholz, M. R., et al. 2021, ApJ, 920, L46
Krause, M. G. H., Charbonnel, C., Bastian, N., & Diehl, R. 2016, A&A, 587, A53
Krause, M. G. H., Offner, S. S. R., Charbonnel, C., et al. 2020, Space Sci. Rev., 216, 64
Kruijssen, J. M. D. 2012, MNRAS, 426, 3008
Kusakabe, H., Verhamme, A., Blaizot, J., et al. 2022, A&A, 660, A44
Langeroodi, D., & Hjorth, J. 2023, arXiv e-prints [arXiv:2307.06336]
Larson, R. B. 1976, MNRAS, 176, 31
Leclercq, F., Bacon, R., Wisotzki, L., et al. 2017, A&A, 608, A8
Leclercq, F., Bacon, R., Verhamme, A., et al. 2020, A&A, 635, A82
Li, Z., Dekel, A., Sarkar, K. C., et al. 2024, A&A, 690, A108
Lotz, J. M., Jonsson, P., Cox, T. J., & Primack, J. R. 2008, MNRAS, 391, 1137
Lovell, C. C., Harrison, I., Harikane, Y., Tacchella, S., & Wilkins, S. M. 2023, MNRAS, 518, 2511
Magnelli, B., Boogaard, L., Decarli, R., et al. 2020, ApJ, 892, 66
Mainali, R., Rigby, J. R., Chisholm, J., et al. 2022, ApJ, 940, 160
Maiolino, R., Scholtz, J., Witstok, J., et al. 2024, Nature, 627, 59
Marques-Chaves, R., Álvarez-Márquez, J., Colina, L., et al. 2020a, MNRAS, 499, L105
Marques-Chaves, R., Pérez-Fournon, I., Shu, Y., et al. 2020b, MNRAS, 492, 1257
Marques-Chaves, R., Schaerer, D., Álvarez-Márquez, J., et al. 2021, MNRAS, 507, 524
Marques-Chaves, R., Schaerer, D., Álvarez-Márquez, J., et al. 2022, MNRAS, 517, 2972
Marques-Chaves, R., Schaerer, D., Kuruvanthodi, A., et al. 2024, A&A, 681, A30
Martin, C. L., Dijkstra, M., Henry, A., et al. 2015, ApJ, 803, 6
Martins, F., & Palacios, A. 2022, A&A, 659, A163
Martins, F., Schaerer, D., Marques-Chaves, R., & Upadhyaya, A. 2023, A&A, 678, A159
Mason, C. A., Trenti, M., & Treu, T. 2023, MNRAS, 521, 497
Matteucci, F. 1994, A&A, 288, 57
Mauerhofer, V., Verhamme, A., Blaizot, J., et al. 2021, A&A, 646, A80
Megeath, S. T., Gutermuth, R., Muzerolle, J., et al. 2016, AJ, 151, 5
Menon, S. H., Federrath, C., & Krumholz, M. R. 2023, MNRAS, 521, 5160
Menon, S. H., Lancaster, L., Burkhart, B., et al. 2024a, ApJ, 967, L28
Menon, S. H., Burkhart, B., Somerville, R. S., Thompson, T. A., & Sternberg, A. 2024b, ApJ, submitted [arXiv:2408.14591]
Messa, M., Dessauges-Zavadsky, M., Richard, J., et al. 2022, MNRAS, 516, 2420
Messa, M., Dessauges-Zavadsky, M., Adamo, A., Richard, J., & Claeyssens, A. 2024, MNRAS, 529, 2162
Meštrić, U., Vanzella, E., Upadhyaya, A., et al. 2023, A&A, 673, A50
Morishita, T., Stiavelli, M., Chary, R.-R., et al. 2024, ApJ, 963, 9
Norris, M. A., Kannappan, S. J., Forbes, D. A., et al. 2014, MNRAS, 443, 1151
Oteo, I., Zwaan, M. A., Ivison, R. J., Smail, I., & Biggs, A. D. 2017, ApJ, 837, 182
Pasha, I., & Miller, T. B. 2023, J. Open Source Softw., 8, 5703
Renzini, A. 2023, MNRAS, 525, L117
Ribeiro, B., Le Fèvre, O., Tasca, L. A. M., et al. 2016, A&A, 593, A22
Rivera-Thorsen, T. E., Dahle, H., Gronke, M., et al. 2017, A&A, 608, L4
Rivera-Thorsen, T. E., Dahle, H., Chisholm, J., et al. 2019, Science, 366, 738
Saldana-Lopez, A., Schaerer, D., Chisholm, J., et al. 2022, A&A, 663, A59
Schaerer, D., Marques-Chaves, R., Xiao, M., & Korber, D. 2024a, A&A, 687, L11
Schaerer, D., Guibert, J., Marques-Chaves, R., & Martins, F. 2024b, A&A, submitted [arXiv:2407.12122]
Senchyna, P., Plat, A., Stark, D. P., et al. 2024, ApJ, 966, 92
Shapley, A. E., Steidel, C. C., Pettini, M., & Adelberger, K. L. 2003, ApJ, 588, 65
Shen, X., Vogelsberger, M., Boylan-Kolchin, M., Tacchella, S., & Kannan, R. 2023, MNRAS, 525, 3254
Smith, B. M., Windhorst, R. A., Jansen, R. A., et al. 2018, ApJ, 853, 191
Stanway, E. R., & Eldridge, J. J. 2018, MNRAS, 479, 75
Steidel, C. C., Erb, D. K., Shapley, A. E., et al. 2010, ApJ, 717, 289
Steidel, C. C., Bogosavljević, M., Shapley, A. E., et al. 2018, ApJ, 869, 123
Tacchella, S., Dekel, A., Carollo, C. M., et al. 2016, MNRAS, 458, 242
Tang, M., Stark, D. P., & Ellis, R. S. 2022, MNRAS, 513, 5211
Thompson, T. A., & Heckman, T. M. 2024, ARA&A, 62, 529
Topping, M. W., Stark, D. P., Senchyna, P., et al. 2024, MNRAS, 529, 3301
Trinca, A., Schneider, R., Valiante, R., et al. 2024, MNRAS, 529, 3563
Upadhyaya, A., Marques-Chaves, R., Schaerer, D., et al. 2024, A&A, 686, A185
van der Wel, A., Bell, E. F., Häussler, B., et al. 2012, ApJS, 203, 24
van Dokkum, P. G., Franx, M., Kriek, M., et al. 2008, ApJ, 677, L5
Vanzella, E., Caminha, G. B., Calura, F., et al. 2020, MNRAS, 491, 1093
Vanzella, E., Castellano, M., Bergamini, P., et al. 2022, A&A, 659, A2
Vanzella, E., Claeyssens, A., Welch, B., et al. 2023, ApJ, 945, 53
Verhamme, A., Dubois, Y., Blaizot, J., et al. 2012, A&A, 546, A111
Verhamme, A., Orlitová, I., Schaerer, D., & Hayes, M. 2015, A&A, 578, A7
Weibel, A., Oesch, P. A., Barrufet, L., et al. 2024, MNRAS, 533, 1808
Williams, H., Kelly, P. L., Chen, W., et al. 2023, Science, 380, 416
Xiao, M., Oesch, P., Elbaz, D., et al. 2023, Nature, submitted [arXiv:2309.02492]
Ziparo, F., Ferrara, A., Sommovigo, L., & Kohandel, M. 2023, MNRAS, 520, 2445
Zolotov, A., Dekel, A., Mandelker, N., et al. 2015, MNRAS, 450, 2327